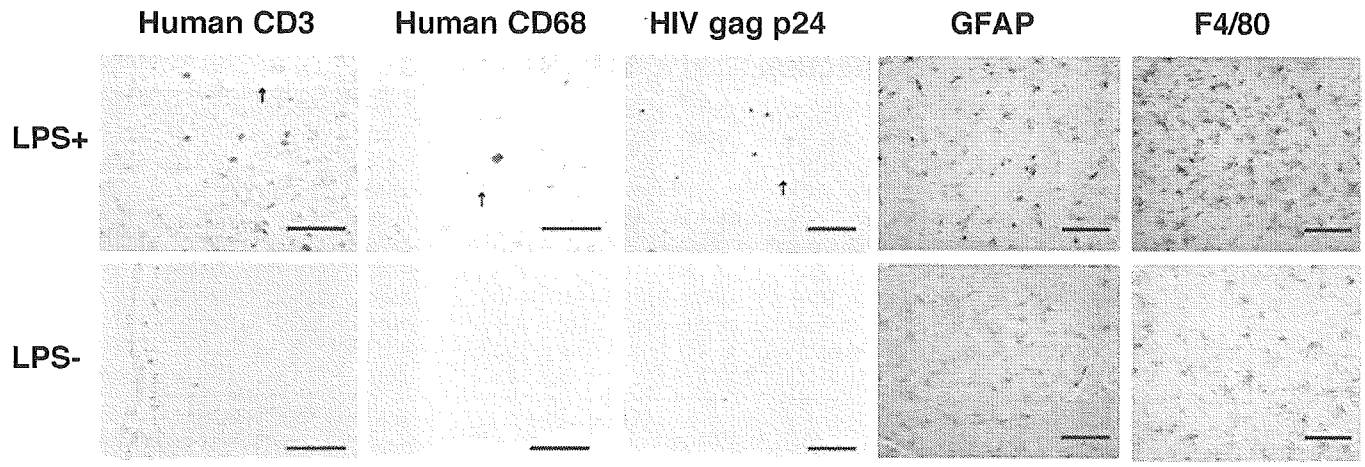

Fig. 1. Migration of human PBMCs after LPS treatment and neuropathology in the brain of HIV-1-infected hu-PBMC-NOD-SCID mice. hu-PBMC-NOD-SCID mice were infected with JRFL and LPS was administered or not 7 days after infection. Three days later, the brains were subjected to immunohistochemical staining. Single staining for the indicated markers of brains from infected mice with or without LPS treatment is shown. Arrows indicate vessels. One representative mouse in Table 1 is shown. (Scale bars, 100 μm.)

$CD3^+$ T cells (91.3 ± 34.4 cps in JRFL-infected brains and 36.0 ± 12.7 cps in NL4-3-infected brains), was found in the brain parenchyma of closed regions to vessels (Fig. 1, arrows) 3 days after LPS treatment (10 days after infection; Fig. 1, Table 1) and 21 days after LPS treatment (data not shown), as compared with the LPS-untreated mice ($P < 0.05$). In contrast, the number of human cells [human leukocyte antigen (HLA)-ABC^+ (HLA^+)] recovered from mouse peritoneal lavages decreased after LPS treatment (213.2 ± 159.7 × 10^4 cells without LPS treatment versus 47.1 ± 37.2 × 10^4 cells with LPS treatment in JRFL-infected mice; Table 1, $P < 0.05$). These infiltrated cells were mainly localized in the perivascular region of cortex, basal ganglia, hippocampus, and cerebellum. We also found an increased number of $GFAP^+$ astrocytes (astrocytosis) and clustering of $F4/80^+$ microglia (microglial nodule) 3 days after LPS treatment in both JRFL- and NL4-3-infected hu-PBMC-NOD-SCID mice, as well as HIV-uninfected hu-PBMC-NOD-SCID and untransplanted NOD-SCID mice, compared with mice that were not treated with LPS (Fig. 1, Table 1), indicating that these features were independent of HIV-1 infection.

Neuronal apoptosis is a hallmark of HIV encephalopathy leading to neuronal dysfunction (6). We examined whether our mouse model had such a feature of the disease. After LPS treatment, histological examination clearly demonstrated apoptosis in the brain. We initially performed TUNEL staining for apoptotic cells. The LPS treatment markedly increased the number of $TUNEL^+$ apoptotic cells (78.8 ± 21.5 cps in JRFL-infected brains and 33.3 ± 9.36 cps in NL4-3-infected brains) in cortex, basal ganglia, hippocampus, and cerebellum of HIV-1 infected hu-PBMC-NOD-SCID mice (Table 1) 3 days after LPS treatment (10 days after infection), compared with the LPS-untreated mice (11.4 ± 5.37 cps in JRFL-infected brains and 10.0 ± 4.24 cps in NL4-3-infected brains; Fig. 2*a*, Table 1). A similar level of increase was also observed 21 days after LPS treatment (28 days after infection; Fig. 2*a*). To identify apoptotic neurons, we next performed FNG staining to label Nissl bodies in the cytoplasm as a neuron-specific marker, along with TUNEL staining (Fig. 2*b*). The FNG stains nucleus of all cells and only cytoplasmic Nissl bodies of neurons. Notably, 10–20% of the $TUNEL^+$ cells were cytoplasmic FNG^+ ($cFNG^+$) neurons (Fig. 2 *b* and *c*), and we observed these only after LPS treatment and only in the JRFL-infected mice (13.1 ± 4.47 cps in JRFL-infected brains, Table 1), not NL4-3-infected mice (Table 1). We further verified the identity of the apoptotic neurons by dual-color staining for TUNEL and another neuron-specific marker, anti-microtubule-associated protein (MAP)-2 (Fig. 2*d*). We also confirmed the apoptosis event in the brain of HIV-1-infected mice by immunostaining using an Ab specific for active form of caspase-3 (Fig. 2*e*). In addition, we found a modest increase in apoptotic cells (25.0 ± 10.8 cps) in the brain of HIV-uninfected hu-PBMC-NOD-SCID mice at 3 days after LPS treatment (Fig. 2*a*, Table 1), but these cells did not include $cFNG^+$ neurons (Table 1) and disappeared at 21 days after LPS treatment (data not shown).

These results indicated that LPS treatment of M-tropic JRFL-infected hu-PBMC-NOD-SCID mice induced some neuropathological changes resembling HIV encephalopathy, especially including infiltration of HIV-infected macrophages and neuronal apoptosis in the brain. In contrast, LPS treatment of T-tropic NL4-3-infected hu-PBMC-NOD-SCID mice induced infiltration of only HIV-infected T cells and apoptosis in nonneuronal cells (Table 1), human T cells, and mouse cells including astrocytes, microglias, and endothelial cells (data not shown). These results indicated that the HIV-infected T cells in the brain were not competent to induce neuronal apoptosis, suggesting a critical role of HIV-infected macrophages. Although this model has limitations, it is possible to examine the mechanism of neuronal damage through invading HIV-1-infected macrophages.

To confirm the requirement of HIV-1-infected macrophage in brain for inducing the neuronal apoptosis, we used recombinant M- (NL-CSFV3-EGFP) and T-tropic (NL-EGFP) HIV-1 expressing GFP as a marker for replicative infection. These recombinant viruses are identical except for the V3 sequence of *env* that determines the tropism. We infected hu-PBMC-NOD-SCID mice with these viruses and administered LPS. A significant level of systemic infection was established, as estimated by HIV gag p24 plasma levels (data not shown). Both 40–50% of $CD68^+$ macrophages and 10–20% of $CD68^-$ $CD3^+$ T cells in the brain were infected (GFP^+) by M-tropic NL-CSFV3-EGFP, whereas 10–20% of $CD68^-$ $CD3^+$ T cells were infected by NL-EGFP in the brain (Fig. 3). We could not find infected (GFP^+) $CD68^+$ macrophages in the brain of NL-EGFP-infected mice. Importantly, apoptotic neurons exhibiting a blue cytoplasm with a pink nucleus, observed by dual-color detection with NeuroTrace blue fluorescent Nissl stain (FNB, blue) and TUNEL (red), were frequently found (10.8 ± 4.97 cps) in the M-tropic virus-infected brain, but not in the T-tropic virus-

MICROBIOLOGY

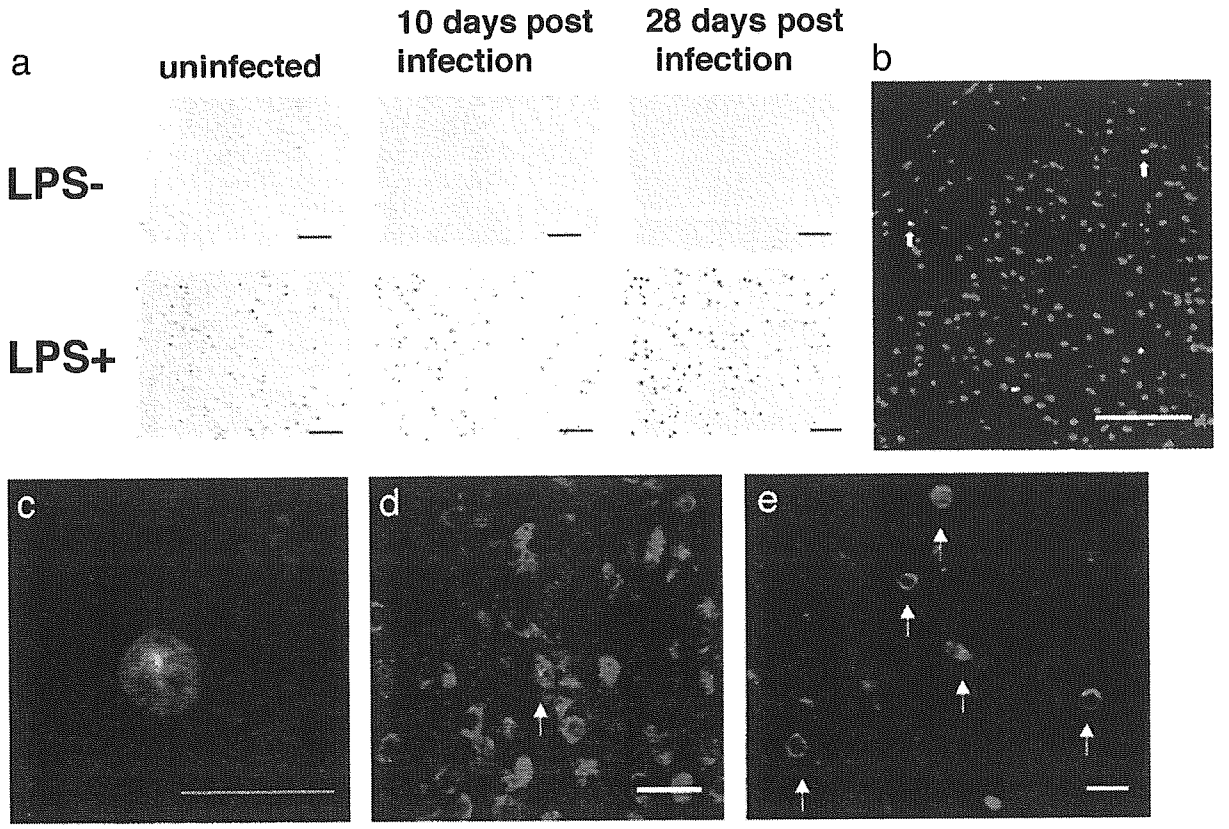

Fig. 2. Apoptosis in the brains of M-tropic HIV-1_{JRFL}-infected hu-PBMC-NOD-SCID mice after LPS treatment. hu-PBMC-NOD-SCID mice were infected with JRFL, and LPS was administered or not 7 days after infection. The brains were subjected to histological staining 3 or 21 days later. (*a*) TUNEL staining of brains from uninfected or infected mice 3 or 21 days later with or without LPS treatment. (Scale bar, 100 μm.) (*b–e*) Apoptotic neurons in the brain of infected mice 3 days after LPS treatment. (*b*) FNG (green)/TUNEL (red) staining (low magnification). Arrows indicate cFNG$^+$ TUNEL$^+$ apoptotic neurons. (Scale bar, 100 μm.) (*c*) FNG (green)/TUNEL (red) staining (high magnification) shows a cFNG$^+$ TUNEL$^+$ neuron. (Scale bar, 20 μm.) (*d*) MAP-2 (green)/TUNEL (red) staining shows a green cytoplasm and a red nucleus. (Scale bar, 20 μm.) (*e*) Active form of caspase-3 (green) staining. Arrows indicate active form of caspase-3$^+$ cells. (Scale bar, 20 μm.)

infected brain (Fig. 3, Table 1). These results further substantiated that the HIV-infected macrophages in the brain were necessary for the induction of neuronal apoptosis.

Critical Contribution of TRAIL to Neuronal Apoptosis. We next explored the molecular mechanism for the HIV-mediated neuronal apoptosis in our model. The expression of TNF-α, IL-1β, TRAIL, and FasL was examined, because these molecules were reportedly expressed in HIV-1-infected macrophages (6, 18, 19). Dual-color staining demonstrated that $\approx$40–60% of the infiltrating human CD68$^+$ macrophages expressed TNF-α, IL-1β, and/or TRAIL, but not FasL (data not shown). In contrast, in the HIV-1-uninfected brain, $\approx$40–50% of the infiltrating human macrophages expressed TNF-α and/or IL-1β, but not TRAIL, after LPS treatment (data not shown). Thus, the expression of TRAIL on infiltrating human macrophages was found to be preferentially augmented in the infected brains after LPS treatment. Furthermore, triple-color analysis after infection with NL-CSFV3-EGFP indicated that TRAIL was expressed in $\approx$50% of HIV-infected CD68$^+$ macrophages and 20% of HIV-infected T cells, whereas TNF-α was expressed in $\approx$80% of HIV-infected CD68$^+$ macrophages and FasL was expressed $\approx$30% of the infected T cells but not in the infected CD68$^+$ macrophages (Fig. 4*a*). Dual-color staining for apoptotic cells by TUNEL and for human CD68, HIV gag p24, or human TRAIL showed that some apoptotic cells were predominantly apposed to HIV-infected macrophages expressing TRAIL but not to HIV-1-infected T cells (Fig. 4*b*). These results suggested that the occurrence of neuronal apoptosis might be associated with the expression of TRAIL in HIV-infected macrophages.

Finally, we examined the contribution of TRAIL, TNF-α, and FasL to the neuronal apoptosis in the brain of JRFL-infected hu-PBMC-NOD-SCID mice by administering neutralizing mAbs against these molecules at the time of LPS treatment. The infiltration of human CD3$^+$ T cells, human CD68$^+$ macrophages,

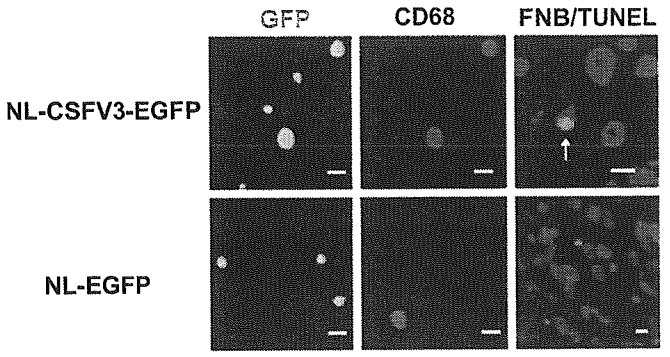

Fig. 3. Association of HIV-1-infected macrophages with neuronal apoptosis. hu-PBMC-NOD-SCID mice were infected with M-tropic NL-CSFV3-EGFP or T-tropic NL-EGFP, and LPS was administered or not 7 days after infection. Brains were retrieved 10 days after infection and subjected to histological analysis for GFP (green) and CD68 (red), or FNB (blue) and TUNEL (red). In FNB/TUNEL staining, cytoplasmic FNB$^+$ (cFNB$^+$) TUNEL$^+$ apoptotic neurons have a blue cytoplasm and a pink nucleus, which is merged with blue and red, as indicated by the arrow. (Scale bars, 10 μm.)

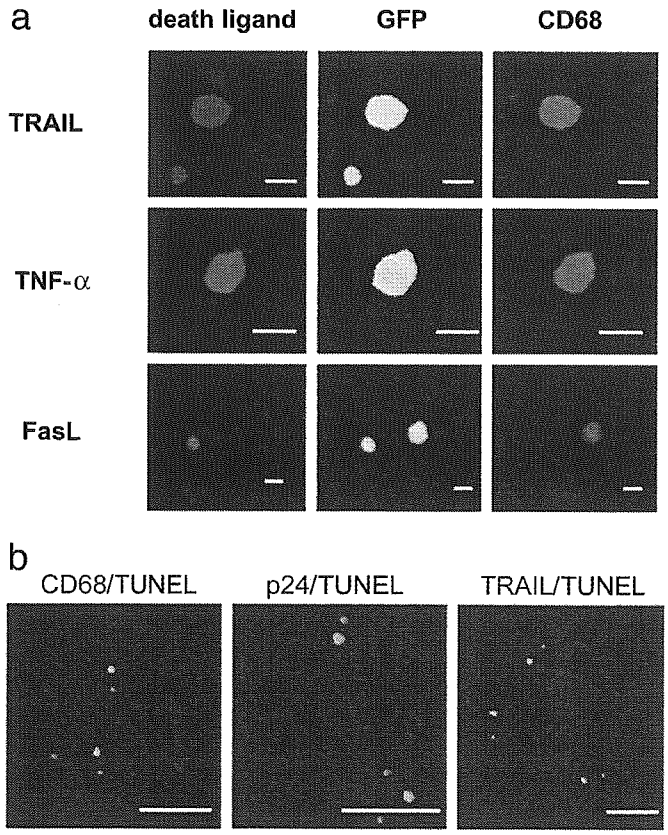

Fig. 4. Association of apoptotic cells with HIV-1-infected macrophages expressing death-inducing molecules. (*a*) Expression of TRAIL, TNF-α, or FasL on HIV-1-infected macrophage. hu-PBMC-NOD-SCID mice were infected with M-tropic NL-CSFV3-EGFP and LPS was given or not 7 days after infection. Three days later, brain sections were subjected to histological analysis for GFP (green), human CD68 (red), and human TRAIL, TNF-α, or FasL (blue) simultaneously. A representative cell is shown. (Scale bars, 10 μm.) (*b*) hu-PBMC-NOD-SCID mice were infected with JRFL, and LPS was given 7 days after infection. Three days later, brain sections were subjected to dual-color staining for human CD68, HIV gag p24, or human TRAIL (green) and TUNEL (red). (Scale bars, 100 μm.)

and HIV gag p24$^+$ cells in the brain was not affected by the administration of these mAbs (data not shown). Neuronal apoptosis was significantly inhibited by the anti-human TRAIL mAb (RIK-2; $P = 0.0005$ by Welch's t test), but not by the anti-human TNF-α mAb (28401.111) or the anti-human FasL mAb (NOK-1), as compared with control mouse IgG (Table 2). These results indicated a critical contribution of human TRAIL to the neuronal apoptosis in the brain of M-tropic HIV-1-infected hu-PBMC-NOD-SCID mice.

Table 2. Inhibition of apoptosis by anti-human TRAIL mAb, TNF-α mAb, or FasL mAb

Ab	*n*	TUNEL$^+$	TUNEL$^+$ cFNG$^+$
Human TRAIL	8	35.0 ± 13.2	0.38 ± 0.34*
Human TNF-α	5	42.8 ± 3.56	5.20 ± 2.59
Human FasL	6	68.3 ± 15.3	9.17 ± 1.47
Control mouse IgG	5	69.4 ± 39.8	8.60 ± 2.07

hu-PBMC-NOD-SCID mice were infected with the JRFL strain of HIV-1 and given LPS and the indicated neutralizing mAb 7 days after infection. Three days later, mice were killed and brains were subjected to histological analyses. Data are indicated as the mean ± SD of the number of TUNEL$^+$ cells and TUNEL$^+$ cFNG$^+$ cells per slice from five to eight mice.
*$P < 0.05$ compared with control mouse IgG by Welch's t test.

Discussion

In the present study, we developed a murine model of the HIV-CNS infection. In HIV-infected hu-PBMC-NOD-SCID mice without LPS treatment, no neuropathological changes excepting sparse astrocytosis were found. On the other hand, LPS treatment significantly induced the migration of HIV-infected T cells and macrophages into brain, along with the appearance of intense astrocytosis and microglial nodule. However, the same levels of astrocytosis and microglial nodules were also induced in uninfected mice with LPS treatment, indicating that these pathological changes did not solely result from HIV infection in brain. Although our murine model was contrived to a model of HIV encephalopathy, we cannot fully address the mechanism. Most importantly, however, neuronal apoptosis was specifically induced in infected brain region through migration of HIV-infected macrophages but not T cells after LPS treatment. Thus, we used this model to explore the cellular and molecular mechanism for the HIV-induced neuronal apoptosis *in vivo*.

Administration of LPS to the HIV-1-infected mice induced infiltration of the HIV-infected human macrophages and T cells into the perivascular region of the brain tissue. This effect of LPS seemed to be mediated by an increased expression of integrin very late antigen 4 (VLA-4) on human macrophages and T cells and an increased expression of vascular cell adhesion molecule 1 (VCAM-1) on the endothelium in the brain (unpublished observation). It has been reported that human VLA-4 could interact with mouse VCAM-1 (20) and that transendothelial migration of human T cells and macrophages was augmented with LPS treatment (21). Consistent with this idea, an increased expression of VCAM-1 has been implicated in the migration of macrophages into the brain during HIV and simian immunodeficiency virus (SIV) infection (22). LPS is an endotoxin produced by Gram-negative bacteria and has a potent stimulatory effect on endothelial cells and macrophages/microglia (23). It has been proposed that some factor associated with advanced HIV infection in the periphery is an important trigger for the infiltration of HIV-infected macrophages into the brain that leads to neuronal apoptosis (6). In fact, increased expression of human leukocyte antigen (HLA)-DR on human T cells and TRAIL and TNF-α on human macrophages was observed after LPS treatment (data not shown). These changes might be induced by activation of macrophages directly by LPS or indirectly by proinflammatory cytokines, such as TNF-α and IL-1β, secreted from these cells. This result suggests that similar changes in patients with HIV encephalopathy may be also mediated by a similar mechanism.

Using this model, we demonstrated that HIV-1 infection in the brain-infiltrating cells is essential for the induction of neuronal apoptosis. Apoptotic neurons were found only in the perivascular region of brains from M-tropic virus-infected mice after LPS treatment. In our mouse model, a large number of CD3$^+$ T cells was also infiltrated into brain tissue coincidentally with infiltration of macrophages. This is apparently different from the pathological feature of HIV-infected human or SIV-infected monkey brain, and may represent a limitation of our mouse model. However, the level of TRAIL expression on HIV-1-infected macrophages in the brain was higher than that on HIV-1-infected T cells, suggesting that the TRAIL molecules expressed on HIV-1-infected macrophages have a critical role in the development of neuronal apoptosis. This requirement of HIV-infected macrophages for neuronal apoptosis is consistent with previous observations in the specimens from HIV encephalopathy patients (2) and in the brains of SCID mice inoculated intracerebrally with HIV-1-infected human macrophages (24). These findings suggest that macrophage activation by HIV

infection itself or by M-tropic viral proteins might induce neurotoxicity. In this respect, it is noteworthy that the infection with a recombinant M-tropic virus (NL-CSFV3-EGFP), but not with a T-tropic virus (NL-EGFP), was neuropathogenic, because these viruses differ only in their V3 sequence of *env*. This result further substantiates that the ability of HIV-1 to infect macrophages plays a key role in the induction of neuronal apoptosis.

We further explored the molecular mechanism for the HIV-infected cell-mediated neuronal apoptosis by using our model. The brain-infiltrating cells expressed TRAIL in an HIV infection-dependent manner, whereas TNF-α and IL-1β were expressed independent of HIV infection after LPS treatment. TRAIL was preferentially expressed in HIV-infected cells especially macrophages, which were apposed to apoptotic neurons (Fig. 4*b*). More important, administration of a neutralizing anti-TRAIL mAb markedly inhibited the neuronal apoptosis in the brain (Table 2). In addition, we recently found significant up-regulation of TRAIL expression on macrophages in brain tissues of HIV encephalopathy patients (Y.M., unpublished data). These results revealed a critical role of TRAIL expressed on HIV-infected cells in neuronal apoptosis. TRAIL expression in HIV-infected cells might be induced by HIV-1 tat, as recently demonstrated (18), or by IFN, as previously demonstrated in peripheral blood monocytes *in vitro* (25). We also confirmed the high level of TRAIL expression on *in vitro* cultured HIV-1-infected, monocyte-derived macrophages (Y.M., unpublished data). The neurotoxic effect of human TRAIL was further verified against primary cultured neuronal/glial cells from fetal mice *in vitro* (Y.M., unpublished data). In this system, however, it remains to be determined whether TRAIL can induce apoptosis in neurons directly or whether it might act indirectly to stimulate glial cells to produce neurotoxic substances such as excitatory amino acids. However, it has been demonstrated that TRAIL directly induced apoptosis for neuronal cells *in vitro* (26). TRAIL-induced apoptosis is controlled by the expression of death-inducing or decoy receptors and intracellular proteins such as c-FLIP (cellular FLICE-inhibitory protein; ref. 27). Furthermore, it has recently been reported that a death-inducing TRAIL receptor was constitutively expressed on neurons (28). Further studies are needed to elucidate the molecular mechanisms for the TRAIL expression in HIV-infected macrophages and the TRAIL-mediated neuronal apoptosis.

In conclusion, this study has shown a critical role of TRAIL expressed on HIV-infected cells for neuronal apoptosis in the CNS of our murine HIV-1-infected model. This result suggests that a similar mechanism may be operative in the pathogenesis of HIV-associated dementia in early stages. We also previously demonstrated a critical contribution of TRAIL to the depletion of HIV-uninfected bystander $CD4^+$ T cells in lymphoid organs, a step leading to AIDS (10). Therefore, TRAIL may be an important target for therapeutic intervention of HIV-associated dementia, as well as AIDS, in HIV-1-infected patients. Further studies in neuropathogenic monkey models are expected to address this possibility.

We thank Profs. K. Sugamura and T. Kitamoto (Tohoku University) for helpful discussions, and T. Ohwada and Y. Numata (Tokyo Medical and Dental University) for technical support and critical advice. This work was supported by grants from the Ministry of Health, Labor, and Welfare and the Ministry of Education, Culture, Sports, Science, and Technology of Japan. Y.K. was supported by the Naito Foundation.

1. Budka, H., Wiley, C. A., Kleihues, P., Artigas, J., Asbury, A. K., Cho, E. S., Cornblath, D. R., Dal Canto, M. C., DeGirolami, U. & Dickson, D. (1991) *Brain Pathol.* **1,** 143–152.
2. Adle-Biassette, H., Levy, Y., Colombel, M., Poron, F., Natchev, S., Keohane, C. & Gray, F. (1995) *Neuropathol. Appl. Neurobiol.* **21,** 218–227.
3. Lipton, S. A. (1997) *Curr. Opin. Neurol.* **10,** 247–253.
4. Koenig, S., Gendelman, H. E., Orenstein, J. M., Dal Canto, M. C., Pezeshkpour, G. H., Yungbluth, M., Janotta, F., Aksamit, A., Martin, M. A. & Fauci, A. S. (1986) *Science* **233,** 1089–1093.
5. Lipton, S. A. & Gendelman, H. E. (1995) *N. Engl. J. Med.* **332,** 934–940.
6. Kaul, M., Garden, G. A. & Lipton, S. A. (2001) *Nature* **410,** 988–994.
7. Prospero-Garcia, O., Gold, L. H., Fox, H. S., Polis, I., Koob, G. F., Bloom, F. E. & Henriksen, S. J. (1996) *Proc. Natl. Acad. Sci. USA* **93,** 14158–14163.
8. Buch, S., Pinson, D., Hou, Y., Adany, I., Li, Z., Mukherjee, S., Jia, F., Mackay, G., Silverstein, P., Kumar, A. & Narayan, O. (2000) *J. Med. Primatol.* **29,** 96–106.
9. Koyanagi, Y., Tanaka, Y., Kira, J., Ito, M., Hioki, K., Misawa, N., Kawano, Y., Yamasaki, K., Tanaka, R., Suzuki, Y., *et al.* (1997) *J. Virol.* **71,** 2417–2424.
10. Miura, Y., Misawa, N., Maeda, N., Inagaki, Y., Tanaka, Y., Ito, M., Kayagaki, N., Yamamoto, N., Yagita, H., Mizusawa, H. & Koyanagi, Y. (2001) *J. Exp. Med.* **193,** 651–660.
11. Koyanagi, Y., Miles, S., Mitsuyasu, R. T., Merrill, J. E., Vinters, H. V. & Chen, I. S. (1987) *Science* **236,** 819–822.
12. Adachi, A., Gendelman, H. E., Koenig, S., Folks, T., Willey, R., Rabson, A. & Martin, M. A. (1986) *J. Virol.* **59,** 284–291.
13. Kayagaki, N., Yamaguchi, N., Nakayama, M., Kawasaki, A., Akiba, H., Okumura, K. & Yagita, H. (1999) *J. Immunol.* **162,** 2639–2647.
14. Kayagaki, N., Kawasaki, A., Ebata, T., Ohmoto, H., Ikeda, S., Inoue, S., Yoshino, K., Okumura, K. & Yagita, H. (1995) *J. Exp. Med.* **182,** 1777–1783.
15. Quinn, B., Toga, A. W., Motamed, S. & Merlic, C. A. (1995) *Neurosci. Lett.* **184,** 169–172.
16. Williams, K. C., Corey, S., Westmoreland, S. V., Pauley, D., Knight, H., deBakker, C., Alvarez, X. & Lackner, A. A. (2001) *J. Exp. Med.* **193,** 905–915.
17. Nottet, H. S., Persidsky, Y., Sasseville, V. G., Nukuna, A. N., Bock, P., Zhai, Q. H., Sharer, L. R., McComb, R. D., Swindells, S., Soderland, C. & Gendelman, H. E. (1996) *J. Immunol.* **156,** 1284–1295.
18. Zhang, M., Li, X., Pang, X., Ding, L., Wood, O., Clouse, K., Hewlett, I. & Dayton, A. I. (2001) *J. Biomed. Sci.* **8,** 290–296.
19. Dockrell, D. H., Badley, A. D., Villacian, J. S., Heppelmann, C. J., Algeciras, A., Ziesmer, S., Yagita, H., Lynch, D. H., Roche, P. C., Leibson, P. J. & Paya, C. V. (1998) *J. Clin. Invest.* **101,** 2394–2405.
20. Hession, C., Moy, P., Tizard, R., Chisholm, P., Williams, C., Wysk, M., Burkly, L., Miyake, K., Kincade, P. & Lobb, R. (1992) *Biochem. Biophys. Res. Commun.* **183,** 163–169.
21. Bereta, J., Bereta, M., Cohen, S. & Cohen, M. C. (1993) *Cell. Immunol.* **147,** 313–330.
22. Sasseville, V. G., Newman, W. A., Lackner, A. A., Smith, M. O., Lausen, N. C., Beall, D. & Ringler, D. J. (1992) *Am. J. Pathol.* **141,** 1021–1030.
23. Ng, Y. K. & Ling, E. A. (1997) *Neurosci. Res.* **28,** 111–118.
24. Persidsky, Y., Limoges, J., McComb, R., Bock, P., Baldwin, T., Tyor, W., Patil, A., Nottet, H. S., Epstein, L., Gelbard, H., *et al.* (1996) *Am. J. Pathol.* **149,** 1027–1053.
25. Griffith, T. S., Wiley, S. R., Kubin, M. Z., Sedger, L. M., Maliszewski, C. R. & Fanger, N. A. (1999) *J. Exp. Med.* **189,** 1343–1354.
26. Nitsch, R., Bechmann, I., Deisz, R. A., Haas, D., Lehmann, T. N., Wendling, U. & Zipp, F. (2000) *Lancet* **356,** 827–828.
27. Sheridan, J. P., Marsters, S. A., Pitti, R. M., Gurney, A., Skubatch, M., Baldwin, D., Ramakrishnan, L., Gray, C. L., Baker, K., Wood, W. I., *et al.* (1997) *Science* **277,** 818–821.
28. Dorr, J., Bechmann, I., Waiczies, S., Aktas, O., Walczak, H., Krammer, P. H., Nitsch, R. & Zipp, F. (2002) *J. Neurosci.* **22,** RC209.

A duodenally absorbable CXC chemokine receptor 4 antagonist, KRH-1636, exhibits a potent and selective anti-HIV-1 activity

Kozi Ichiyama*†, Sei Yokoyama-Kumakura†‡, Yuetsu Tanaka†§, Reiko Tanaka§, Kunitaka Hirose‡, Kenji Bannai‡, Takeo Edamatsu‡, Mikiro Yanaka‡, Yoshiaki Niitani‡, Naoko Miyano-Kurosaki¶, Hiroshi Takaku¶, Yoshio Koyanagi‖, and Naoki Yamamoto*,**

*Department of Molecular Virology, Bio-Response, Graduate School, Tokyo Medical and Dental University, Tokyo 113-8519, Japan; ‡Biomedical Research Laboratories, Kureha Chemical Industry Co. Ltd., Tokyo 169-8503, Japan; §Department of Infectious Disease and Immunology, Okinawa-Asia Research Center of Medical Science, University of the Ryukyus, Nishihara-cho, Okinawa 903-0215, Japan; ¶Department of Industrial Chemistry and High Technology Research Center, Chiba Institute of Technology, Narashino, Chiba 275-0016, Japan; and ‖Department of Virology, Tohoku University School of Medicine, Sendai, Miyagi 980-8575, Japan

Communicated by Pedro M. Cuatrecasas, University of California at San Diego School of Medicine, La Jolla, CA, January 23, 2003 (received for review September 4, 2001)

A low molecular weight nonpeptide compound, KRH-1636, efficiently blocked replication of various T cell line-tropic (X4) HIV type 1 (HIV-1) in MT-4 cells and peripheral blood mononuclear cells through the inhibition of viral entry and membrane fusion via the CXC chemokine receptor (CXCR)4 coreceptor but not via CC chemokine receptor 5. It also inhibited binding of the CXC chemokine, stromal cell-derived factor 1α, to CXCR4 specifically and subsequent signal transduction. KRH-1636 prevented monoclonal antibodies from binding to CXCR4 without down-modulation of the coreceptor. The inhibitory effect against X4 viral replication by KRH-1636 was clearly reproduced in the human peripheral blood lymphocyte/severe combined immunodeficiency mouse system. Furthermore, this compound was absorbed into the blood after intraduodenal administration as judged by anti-HIV-1 activity and liquid chromatography MS in the plasma. Thus, KRH-1636 seems to be a promising agent for the treatment of HIV-1 infection.

To date, highly active antiretroviral therapy for HIV type 1 (HIV-1) has led to a dramatic effect in reduction of the extent of viral load, improvement of $CD4^+$ T cell number status, and often remarkable recovery from disease in infected individuals (1–4). However, due to many factors such as the possible appearance of drug-resistant mutants, side effects, and high cost, there is still a great need for improved therapies.

CXC chemokine receptor (CXCR)4 is a coreceptor for the entry of T cell line-tropic (X4) strains of HIV-1, and CC chemokine receptor (CCR)5 serves as a coreceptor for macrophage-tropic (R5) strains of HIV-1 (5–8). In addition, the CXC chemokine stromal cell-derived factor 1α (SDF-1α) blocks the infection of lymphocytes by X4 HIV-1 isolates (9, 10), and the CC chemokines regulated on activation, normal T cells expressed and secreted (RANTES), macrophage inflammatory protein (MIP)-1α, and MIP-1β, which are ligands for CCR5, inhibit the infection of R5 HIV-1 isolates (11). These observations suggest that chemokines or chemokine derivatives or small-molecule chemokine receptor antagonists or agonists may be useful for the treatment of HIV-1 infection. Indeed, several groups of low molecular weight compounds are reported to inhibit HIV-1 infection, including the bicyclam AMD3100 (12–14) and 18-mer peptide T22 (15, 16), which potently block HIV-1 entry and infection through CXCR4. More recently, a nonpeptide small molecular weight compound named TAK-779 was found to be a potent and selective CCR5 antagonist (17). Unfortunately, it is not possible to administer these compounds by the oral route. We believe that oral availability is one of the key issues to be achieved for anti-HIV drugs for the benefit of HIV-1-infected individuals, because HIV-1 infection is chronic and life-long. We therefore focused on the development of orally available chemokine antagonists. This study describes the discovery of a potent CXCR4 antagonist with a small nonpeptide molecule that can be administered orally.

Materials and Methods

Compounds. The synthesis and purification of KRH-1636, *N*-{(*S*)-4-guanidino-1-[(*S*)-1-naphthalen-1-yl-ethylcarbamoyl]butyl}-4-{[(pyridin-2-yl-methyl)amino]methyl}benzamide (Fig. 1*a*), its methansulfonated analog, and AMD3100 were carried out at Kureha Chemical Industry (Tokyo). These compounds were dissolved in dimethyl sulfoxide at 10 mM to exclude any antiviral or cytotoxic effect of dimethyl sulfoxide. T22 was kindly supplied from Seikagaku Kogyo (Tokyo).

Cells. MT-4, MOLT-4, and MOLT-4/HIV-1 human T cell leukemia virus (HTLV)-IIIB cells were maintained in RPMI medium 1640 supplemented with 10% FCS and antibiotics (100 μg/ml penicillin/100 μg/ml streptomycin). Chemokine receptor-expressing human osteosarcoma (HOS) cells were kindly provided by H. Hoshino (Gunma University, Maebashi, Japan) and maintained in DMEM supplemented with 10% FCS and antibiotics. Peripheral blood mononuclear cells (PBMCs) from HIV-1-seronegative healthy donors were isolated by density gradient centrifugation, grown in RPMI medium 1640 supplemented with 10% FCS, and activated with either 1 μg/ml phytohemagglutinin (PHA, Sigma–Aldrich) for 3 days or anti-CD3/CD28 monoclonal antibodies in the presence of IL-2 (20 units/ml, Shionogi, Osaka) at 37°C.

Viruses. The X4 HIV-1 strains IIIB and NL4-3 were obtained from the culture supernatant of MOLT-4/HTLV-IIIB cells and COS-1 cells transfected with a molecular clone, respectively, as described (18, 19). Aliquots of the viral stocks were stored at −80°C until use. The titer of the virus stocks was determined by endpoint titration of 5-fold limiting dilution in quadruplicate on MT-4 cells. Several clinical isolates including X4 (YU-6, YU-10, and YU-11) (20) and R5 strains (YU-1 and YU-2) (21) were propagated in peripheral blood lymphocytes (PBLs) after PHA stimulation.

Immunofluoresence. $CD4^+$ T cells from a normal donor were activated with anti-CD3/CD28 monoclonal antibody-bound magnetic beads in human recombinant IL-2 (rIL-2)/10% FCS contain-

Abbreviations: HIV-1, HIV type 1; CCR, CC chemokine receptor; CXCR, CXC chemokine receptor; SDF-1α, stromal cell-derived factor 1α; HOS, human osteosarcoma; HTLV, human T cell leukemia virus; PBMC, peripheral blood mononuclear cell; PHA, phytohemagglutinin; PBL, peripheral blood lymphocyte; rIL-2, recombinant IL-2; MTT, 3-(4,5-dimethylthiazol-2-yl)-3,5-diphenylformazan; CHO, Chinese hamster ovary; SCID, severe combined immunodeficiency; ECL, extracellular loop.

†K.I., S.Y.-K., and Y.T. contributed equally to this work.

**To whom correspondence should be addressed. E-mail: yamamoto.mmb@tmd.ac.jp.

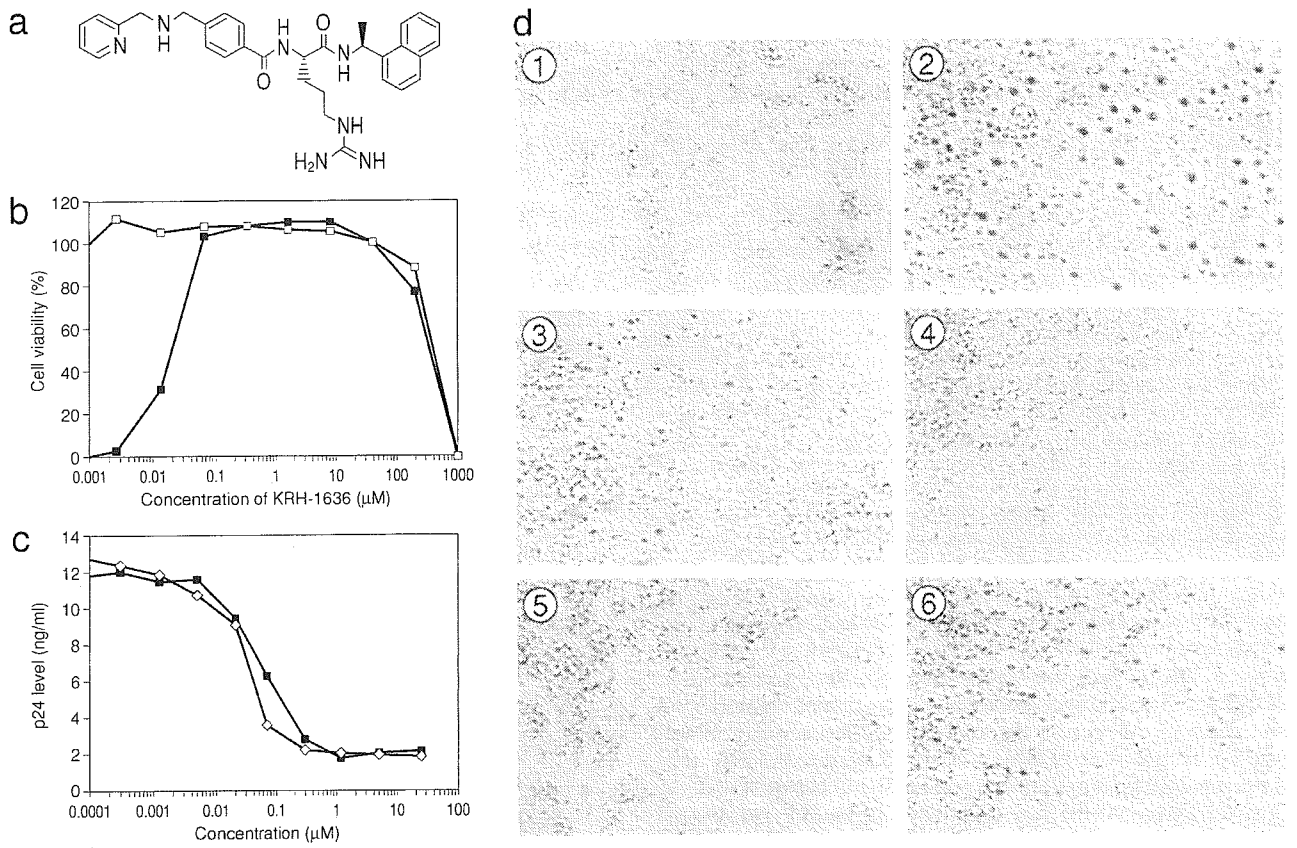

Fig. 1. The chemical structure of the CXCR4 antagonist, KRH-1636, and its anti-HIV-1 activity. (*a*) The chemical structure of KRH-1636. (*b*) Anti-HIV-1 activity of KRH-1636 in MT-4 cells as measured by MTT assay. HTLV-IIIB HIV-1 was used in this study (–□–, mock-infected; –■–, HIV-1). (*c*) Anti-HIV-1 (NL4-3) activity of KRH-1636 in anti-CD3/CD28-stimulated PBMCs as determined by p24 assay. –■–, KRH-1636; –◇–, AMD3100. (*d*) Inhibition of cell fusion by KRH-1636. ①, MOLT-4 cells; ②, coculture; ③, 5 μM KRH-1636; ④, 0.5 μM KRH-1636; ⑤, 0.05 μM KRH-1636; ⑥, 0.005 μM KRH-1636.

ing RPMI medium 1640 for 7 days. These activated cells were treated with 10 μM AMD3100 or KRH-1636 in the IL-2-containing medium at 37°C for 1 h. After washing with cold PBS containing 2% FCS and 0.1% NaN3 [fluorescence-activated cell sorting (FACS) buffer], the cells were pretreated with normal human IgG at 0.1 mg/ml in FACS buffer for 15 min on ice to block the Fc receptors and then stained directly with 12G5-phycoerythrin (PharMingen) for 30 min or indirectly with rat IgG1 monoclonal antibodies A145, A80 (22) and T227 at 5 μg/ml for 30 min followed by goat anti-rat IgG-FITC (DAKO) treatment for 30 min on ice. After washing, the cells were fixed with 1% paraformaldehyde in FACS buffer for 5 min at room temperature and then analyzed on FACSCalibur (Becton Dickinson), a flow cytometer, with CELLQUEST software (Becton Dickinson). The area of positivity was determined by using an isotype-matched mouse monoclonal antibody (Beckman Coulter) and a rat monoclonal antibody against hepatitis C virus, Mo8 of IgG1 isotype (23).

***In Vitro* Anti-HIV-1 Assays.** The 3-(4,5-dimethylthiazol-2-yl)-3,5-diphenylformazan (MTT, Sigma–Aldrich) assay using MT-4 cells was carried out as described (24, 25). For the p24 accumulation assays, PHA-stimulated PBMCs were infected with HIV-1 in the presence of various concentrations of the test compounds unless otherwise stated (16).

Fusion Assay. MOLT-4 and MOLT-4/HIV-1 HTLV-IIIB cells were cocultured for 1 day as described (26).

DNA Construct and Transfection. Human cDNAs for CCR3 (27), CCR4 (28), CCR5 (29), and CXCR1 (30) were amplified by PCR from a human PHA-stimulated PBMC cDNA library and cloned into the pcDNA3.1(+) expression vector with cytomegalovirus promoter (Invitrogen). Transfection was performed with Chinese hamster ovary (CHO) cells by using Lipofectamine (Life Technologies, Grand Island, NY), and stable transfectants were selected in the presence of 600 μg/ml geneticin (Life Technologies).

Ligand-Binding Assays. MT-4, CHO, or chemokine receptor-expressing CHO cells (5×10^6 cells per 0.2 ml per well) were cultured in a 24-well microtiter plate. After 24 h of incubation at 37°C, culture medium was replaced with binding buffer (RPMI medium 1640 supplemented with 0.1% BSA). Binding reactions were performed on ice for 2 h in the presence of [^{125}I]SDF-1α [Daiichi Kagaku Yakuhin, Tokyo; specific activity, 2,200 Ci/mmol (1 Ci = 37 GBq)] and various concentrations of the test compound. The binding reaction was terminated by washing out the free ligand with cold PBS, and the cell-associated radioactivities were counted by using a scintillation counter (Packard Japan, Tokyo).

Coreceptor-Mediated Ca^{2+} Signaling. Fura2-acetoxymethyl ester-loaded HOS/CXCR4 cells were incubated in the absence or presence of various concentrations of KRH-1636. Changes in the intracellular Ca^{2+} level in response to SDF-1α (1 μg/ml) were determined by using a fluorescence spectrophotometer.

Infection of Human PBL/Severe Combined Immunodeficiency (SCID) Mice. Female C.B-17 SCID mice were purchased from CLEA Japan (Tokyo). i.p. and intrasplenic cell transfers were performed on 6- to 8-week-old mice. SCID mice were depleted of natural killer cells by i.p. injection with TMβ-1 rat anti-mouse

IL-2Rβ monoclonal antibody (31) (1 mg per animal). After 1 day, 1×10^7 human PBMCs were introduced into the peritoneum together with human rIL-4 (0.4 μg per animal; PeproTech, Rocky Hill, NJ). On the next day, KRH-1636 (0.1 ml of 2 mM solution per animal) or control (0.1 ml of medium alone) was administered i.p. The NL4-3 strain of HIV-1 (0.2 ml of 1×10^4 tissue culture 50% infective dose per milliliter of stock) was infected i.p. On days 1–7 after infection, the same dosage of KRH-1636 or medium was administered i.p. On days 1, 3, 5, and 7 after infection, 0.4 μg of rIL-4 was also administered i.p. On day 9 after infection, plasma and peritoneal lavage fluid (4 ml) were collected and assayed for HIV-1 p24 with an ELISA kit. At the same time, $CD4^+$ and $CD8^+$ T cell numbers were counted.

For the intrasplenic inoculation, 1.5×10^6 PBMCs were transplanted into spleen together with human rIL-4 (0.4 μg) 2 days after TMβ-1 treatment. On the same day, KRH-1636 (0.1 ml of 2 mM solution per animal) or control (0.1 ml of medium alone) was injected i.p. After 1 day, mice were challenged i.p. with the NL4-3 strain of HIV-1 (0.2 ml of 1×10^4 tissue culture 50% infective dose per milliliter of stock). On days 1–4 after infection, mice were administered i.p. with repeated doses of KRH-1636 or medium. On day 4 after infection, 0.2 μg of rIL-4 was also inoculated i.p. On day 12 after infection, plasma and peritoneal lavage fluid (4 ml) were collected and assayed for HIV-1 p24.

A short-term *in vivo* test was performed. Mice were treated with TMβ-1. Twenty-four hours later, they were treated with KRH-1636 (0.2 ml i.p.) for 30 min. Animals then were administered i.p. with 4×10^6 PBMCs activated with anti-CD3/anti-CD28 antibody for 6 days and subsequently infected with HIV-1 ($1–2 \times 10^3$ tissue culture 50% infective dose per 0.1–0.2 ml i.p.) for 2 h. Cells in peritoneal lavage fluid were collected and cultured in IL-2 (20 units/ml)-containing medium. Nine days after culture, p24 assay was performed on culture supernatants.

Detection of KRH-1636 in the Blood After Intraduodenal Administration. Male Wistar rats (6 weeks old, CLEA Japan) were used for *in vivo* studies. KRH-1636 or methansulfonated KRH-1636 was dissolved in 45% hydroxypropyl-β-cyclodextrin. After acclimation for at least 1 week, the rats were fasted for ≈18 h before KRH-1636 administration, anesthetized with diethyl ether, and then pylorus ligated. KRH-1636 was administered into the duodenum through a tube at the dose of 200 mg/ml per kg (two rats for KRH-1636 and three rats for methansulfonated KRH-1636). Blood samples were taken from cervic-venous by using a heparin-treated syringe at 0.25, 0.5, 1, 2, 4, and 6 h after administration and centrifuged to separate the plasma. Next, 100 μl of the plasma was mixed with 400 μl of 0.1% formic acid/methanol. After centrifugation (Kubota, Tokyo) at 15,000 rpm for 5 min, the supernatant was evaporated to dryness under the stream of nitrogen, and samples were dissolved in 25% acetonitrile/0.1% formic acid solution and analyzed by the liquid chromatography mass spectroscope QP8000α (Shimadzu). Anti-HIV-1 activity in serial diluted rat serum with complete medium was measured by an MTT assay using MT-4 cells.

Results

KRH-1636 Is a Potent and Selective Inhibitor of X4 HIV-1. More than 1,000 compounds from the chemical library of Kureha Chemical Industry were surveyed for anti-HIV-1 activity by the conventional MTT assay using $CXCR4^+$ MT-4 cells. Through optimization of the lead compound, we found KRH-1636 (Fig. 1*a*) to be an extremely potent inhibitor of HIV-1 replication in MT-4 cells. The chemistry will be described elsewhere. KRH-1636 completely inhibited X4 HIV-1 (IIIB strain) replication in MT-4 cells at a concentration as low as 0.06 μM (Fig. 1*b*). Its 50% and 90% effective concentrations (EC_{50} and EC_{90}) were 0.0193 and 0.0478 μM, respectively. The 50% cytotoxic concentration (CC_{50}) of KRH-1636 was 406.21 μM when MT-4 cells were used. Thus, the selectivity index (ratio of CC_{50} to EC_{50}) of KRH-1636 was >10,000, indicating that this compound is extremely potent and selective.

Table 1. Anti-HIV-1 activity of KRH-1636 in PBMCs

Virus	Tropism	Compound	EC_{50}, μM
NL4-3	X4	KRH-1636	0.042
		AMD3100	0.022
HTLV-III B	X4	KRH-1636	0.018
		AMD3100	0.016
YU-6	X4	KRH-1636	0.046
YU-10	X4	KRH-1636	0.152
YU-11	X4	KRH-1636	0.025
YU-1	R5	KRH-1636	>10
YU-2	R5	KRH-1636	>2

PHA-stimulated PBMCs were infected with X4- or R5-type HIV-1 strains in the presence of various concentrations of compounds. p24 was monitored 5 days after infection.

The inhibitory activity of KRH-1636 against X4 HIV-1 (NL4-3) replication in PBMCs was also demonstrated by a p24 accumulation assay of culture supernatants of the cells infected with the virus. KRH-1636 (0.0003–20 μM) reduced the antigen levels in a dose-dependent fashion at any time point (Fig. 1*c*). KRH-1636 was also effective against HTLV-IIIB and three clinical isolates including YU-6 (20), YU-10, and YU-11 and showed a similar potency of action to that observed with the NL4-3 strain (Table 1). In contrast, KRH-1636 was ineffective against R5 HIV-1, YU-1, YU-2 (ref. 21; Table 1), and envelope-modified NL4-3 (data not shown) infection in PBMCs. The specific CXCR4 inhibitors, T22 and AMD3100, completely inhibited replication of the IIIB strain at 0.3 and 0.28 μM, respectively, although they did not inhibit replication of the R5 HIV-1 Ba-L strain at concentrations up to 100 μM (data not shown).

KRH-1636 apparently inhibited syncytium formation between MOLT-4 and its HIV-1-converted MOLT-4 cells (Fig. 1*d*). This indicated that KRH-1636 exerted its effect at the initial step of HIV-1 infection such as viral entry and membrane fusion in the target cells.

All these data show that the effect of KRH-1636 is very similar to that of T22 and AMD3100 and strongly suggest that KRH-1636 might interfere with CXCR4 function as a coreceptor.

KRH-1636 Inhibits Ligand Binding to CXCR4. To investigate whether KRH-1636 exerts its effect as a CXCR4 antagonist, the inhibitory effect of the compound on ligand binding to the coreceptor was studied by using MT-4 cells, which express CXCR4 spontaneously. The result showed that [^{125}I]SDF-1α binding was efficiently and dose-dependently suppressed, showing the IC_{50} of KRH-1636 (Fig. 2*a*) and control AMD3100 to be 0.013 μM and 0.068 μM, respectively. To determine whether the inhibitory effect of KRH-1636 on chemokine binding is specific to CXCR4, the activity of KRH-1636 was examined in CHO cells stably expressing CXCR1, CCR3, CCR4, or CCR5. This compound had no effect on the binding of [^{125}I]IL-8, [^{125}I]eotaxin, [^{125}I]TARC (thymus- and activation-regulated chemokine), or [^{125}I]RANTES to CXCR1, CCR3, CCR4, and CCR5, respectively (Fig. 2*a*). These data clearly demonstrate that KRH-1636 selectively inhibits the binding of SDF-1α to CXCR4.

KRH-1636 Inhibits CXCR4-Mediated Ca^{2+} Signaling. In chemokine-induced Ca^{2+}-mobilization experiments, SDF-1α clearly increased the intracellular Ca^{2+} level in HOS/CXCR4 cells at the concentration of 1 μg/ml (Fig. 2*b*). The addition of 10 μM KRH-1636 did not affect the Ca^{2+} level but strongly abrogated the SDF-1α-induced increase in the intracellular Ca^{2+} level of HOS/CXCR4 cells, and the effect was dose-dependent (Fig. 2*b*).

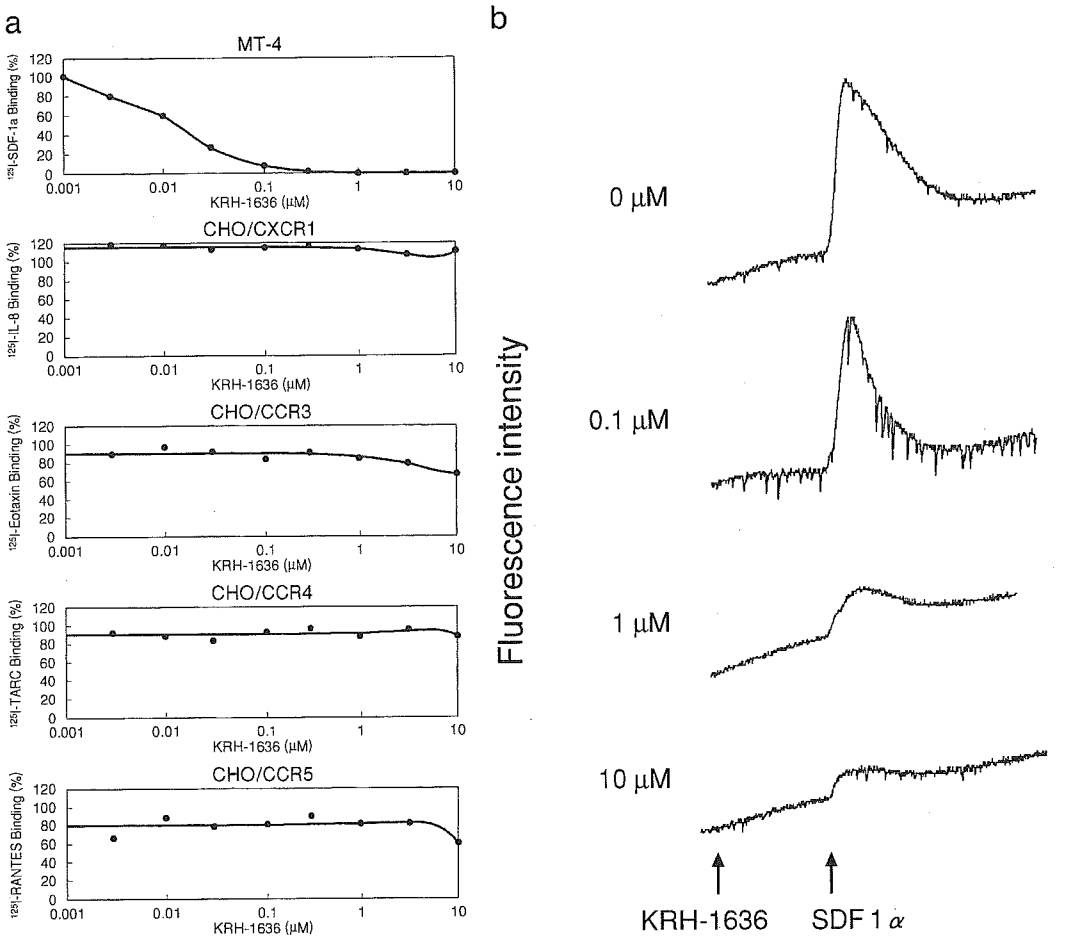

Fig. 2. Inhibitory effects of KRH-1636 on chemokine binding to the cells and SDF-1α-induced Ca^{2+} mobilization in HOS/CXCR4 cells. (*a*) Inhibitory effects of KRH-1636 on chemokine binding to MT-4 or CXCR1-, CCR3-, CCR4-, or CCR5-expressing CHO cells. The percent binding was calculated as 100 × [(binding with inhibitor − nonspecific binding)/(binding without inhibitor − nonspecific binding)]. TARC, thymus- and activation-regulated chemokine. (*b*) Inhibitory effect of KRH-1636 on SDF-1α-induced Ca^{2+} mobilization in HOS/CXCR4 cells.

In contrast, this compound did not affect the Ca^{2+} mobilization induced by RANTES, MCP-1, eotaxin, macrophage-derived chemokine, and MIP-1α in HOS/CCR1, HOS/CCR2b, HOS/CCR3, HOS/CCR4, and HOS/CCR5 cells, respectively, even at the concentration of 10 μM (data not shown). These results indicate that KRH-1636 selectively blocks CXCR4-mediated Ca^{2+} signaling.

Interaction of KRH-1636 with CXCR4. We used four different kinds of monoclonal antibodies, 12G5 [anti-CXCR4, HIV-neutralizing, recognizing its extracellular loop (ECL)1 and -2], A145 (anti-CXCR4, recognizing its N terminus), A80 (anti-CXCR4, HIV-enhancing, recognizing its ECL3), and T227 (anti-CCR5), to study the interaction of KRH-1636 with CXCR4. The binding of 12G5 and A80 but not A145 and T227 monoclonal antibodies to CD3-activated T cells was inhibited dramatically by KRH-1636 (Fig. 4, which is published as supporting information on the PNAS web site, www.pnas.org). Interestingly, the control antagonist AMD3100 showed a similar result. From these data it is strongly suggested that KRH-1636 inhibited the binding of 12G5 and A80 to CXCR4 without inducing down-modulation of the CXCR4 molecule or affecting CCR5 expression.

KRH-1636 Blocks X4 HIV-1 Replication in Human PBL/SCID Mice. KRH-1636 was examined to determine whether it inhibits X4 viral replication *in vivo*. For this, we used both long-term and short-term *in vivo* assays with human PBL/SCID mice. For the long-term tests we applied two different systems in which human PBL/SCID mice were constructed by either an i.p. or intrasplenic inoculation of PBMCs. Because the effect of X4 virus (NL4-3) infection is not as clear as that of R5 virus infection in human PBL/SCID mice, C.B-17 mice were treated with human rIL-4 during the infection period to enhance the replication of X4 HIV-1 (see *Materials and Methods*). The amounts of p24 in peritoneal lavage fluid in five of seven animals with PBMCs that were inoculated i.p. were below the detectable level in KRH-1636-treated mice 9 days after infection, whereas viremia was noted in all seven untreated mice (Table 2). However, a decrease in HIV-1-infected $CD4^+$ T cell number was not clear in untreated mice under the present experimental condition (data not shown). Similarly, the amounts of p24 in the plasma and peritoneal lavage in two animals with PBMCs that were given intrasplenically were below the detectable level in KRH-1636-treated mice after infection, whereas viremia was noted in three untreated mice (data not shown). In a short-term *in vivo* test, KRH-1636 clearly inhibited viral replication and HIV-1-induced $CD4^+$ T cell decrease as observed in the *in vitro* assays (Table 3).

KRH-1636 Is Absorbed Efficiently from the Duodenum into the Blood. Finally, the absorbability of KRH-1636 was investigated by using rats as described in *Materials and Methods*. The concentration of KRH-1636 in plasma or serum was monitored by liquid chromatography MS (plasma) and anti-HIV-1 activity (serum) after in-

Table 2. Anti-HIV-1 effects of KRH-1636 in human PBL-SCID mice as assessed by the long-term *in vivo* test

Mouse	Infected with	Treated with	P24 level, pg/ml	
			Plasma	P.L.*
1	Mock	Medium	<2	<2
2	Mock	KRH-1636†	<2	<2
3	NL4-3	Medium	<2	4.1
4	NL4-3	Medium	<2	5.6
5	NL4-3	Medium	8.4	28.2
6	NL4-3	Medium	12.9	14.9
7	NL4-3	Medium	10.3	180.2
8	NL4-3	Medium	4.4	20.7
9	NL4-3	Medium	<2	8.5
10	NL4-3	KRH-1636	<2	<2
11	NL4-3	KRH-1636	<2	<2
12	NL4-3	KRH-1636	<2	<2
13	NL4-3	KRH-1636	<2	<2
14	NL4-3	KRH-1636	<2	<2
15	NL4-3	KRH-1636	6.9	14.6
16	NL4-3	KRH-1636	17.8	29.5

Mice were inoculated with PBMCs intraperitoneally.
*Peritoneal lavage.
†2 mM, 0.1 ml.

traduodenal administration. To increase the drug availability, the methansulfonated analog of KRH-1636 was also synthesized and studied in a similar manner. The results showed that these compounds were absorbed efficiently from the duodenum of the rats (Fig. 3, *a* for KRH-1636 and *b* for methansulfonated KRH-1636). The bioavailability of KRH-1636 and methansulfonated KRH-1636 in this experiment was estimated to be ≈7% and 69%, respectively, by liquid chromatography MS. Moreover, EC_{50} (%) and EC_{90} (%) of serum at 60 min after the administration of KRH-1636 was 0.18 and 0.27, respectively, as determined by the MTT assay using MT-4 cells (Fig. 3*c*). In this experiment, the concentration of KRH-1636 in plasma at 60 min after administration was 30.6 μM. Therefore, the concentration of KRH-1636 in the blood reached levels that are inhibitory to HIV replication.

Discussion

This report demonstrates a duodenally absorbable CXCR4 antagonist, KRH-1636, that has a potent anti-HIV activity both *in vivo* and *in vitro*.

KRH-1636 selectively inhibited infection of T cell line-tropic X4 virus strains including several clinical isolates without affecting R5 HIV-1. Macrophage-tropic R5 virus strains are isolated from individuals shortly after seroconversion and, during the asymptomatic period of the disease, seem to be responsible for sexual and parenteral transmission and represent the most prevalent phenotype (32, 33). In contrast, X4 HIV-1 isolates tend to appear in infected individuals at the later stages of infection during transition from the asymptomatic to symptomatic state and may be involved in the rapid decline of $CD4^+$ T lymphocytes and progression to AIDS due to strong cytopathicity (34). It therefore is important to find therapies to inhibit CXCR4-mediated infection by X4 HIV-1 to block progression to AIDS.

Table 3. Anti-HIV-1 effects of KRH-1636 in human PBL-SCID mice as assessed by the short-term *in vivo* test

Mouse	Treated with	$CD4^+$T cells ($\times 10^4$)	p24 level, pg/ml
1	Medium	1.3	107
2	Medium	4.4	2,295
3	Medium	3.8	1,326
4	KRH-1636*	37.5	<5
5	KRH-1636	0.8	<5
6	KRH-1636	10.1	<5
7	KRH-1636	17.1	<5
8	KRH-1636	60.2	<5

Cells in peritoneal lavage fluid were collected and cultured in IL-2-containing medium, and a p24 assay was performed 9 days after culture.
*0.1 mM, 0.2 ml.

The inhibition of chemokine receptors by KRH-1636 seemed to be specific to CXCR4 because KRH-1636 was highly inhibitory to the binding of $[^{125}I]$SDF-1α to MT-4 cells (Fig. 2*a*). Furthermore, chemokines binding to CXCR1, CCR3, CCR4, or CCR5 was not inhibited by this compound. Therefore, the inhibitory effect of KRH-1636 was shown to be selective for CXCR4. The inhibitory effects of KRH-1636 on the binding of monoclonal antibodies to CXCR4 (Fig. 4) also support this notion. The specificity of KRH-1636 to CXCR4 seems extremely important from a chemotherapeutic viewpoint, because nonspecific inhibition of β-chemokine receptors may generate serious side effects associated with chemokine dysregulation.

Similar to AMD3100, KRH-1636 did not induce the internalization of CXCR4 (Fig. 4). However, KRH-1636 suppressed the binding of the anti-CXCR4 antibodies, A80 and 12G5, to activated $CD4^+$ T cells. Because these monoclonal antibodies are directed to the different ECLs of the seven-transmembrane receptor CXCR4, it is possible that KRH-1636 may interact with all three ECLs. Alternatively, KRH-1636 may induce a conformational change in the CXCR4 after binding to a distinct site of coreceptor. The exact site on the CXCR4 molecule targeted by this compound remains to be determined.

Oral availability remains one of the key goals to be attained as an anti-HIV drug, because retroviral infection continues throughout the life of infected people. Thus, oral administration of KRH-1636 was conducted in rats and SCID mice (data not shown), the plasma concentrations of the compound and pharmacokinetic parameters of which were determined. Although no measurable absorption of the currently available chemokine receptor antagonists has been reported, substantial transfer not only as a chemical but also as an active anti-HIV compound from the gastrointestinal tract to the blood was achieved with KRH-1636. Further improvement of oral availability and increased penetration into the central nervous system is needed.

C.B-17 SCID mice exhibit multiple immunological defects, and it has been demonstrated that this mutant strain efficiently receives human PBLs (35). After infection, R5-type HIV-1, including JR-CSF and NFN-SX strains, could replicate very efficiently in association with the apparent $CD4^+$ T cell depletion. However, X4 virus does not replicate well in this system, and therefore $CD4^+$ T cell decline is not obvious (36). To overcome this problem, the mice were treated with human IL-4 because our preliminary result showed that X4 virus strains favor the T helper 2-dominant status for their replication and induction of $CD4^+$ T cell decline (37). Our studies clearly showed the *in vivo* inhibitory effect of KRH-1636 on the replication of X4 virus. Although this study was conducted by using an i.p. injection of the compound, oral administration should be effective, because oral bioavailability and efficient adsorption of this compound have been confirmed in rats and the SCID mouse system as well.

Several questions remain to be answered concerning the clinical outcome of coreceptor-based therapy (38). Will blocking of normal CXCR4 function caused by treatment with antagonists be tolerated? In the case of CCR5 antagonists, it will be safe because of the lack of reported immunological disorders in individuals with CCR5Δ32 homozygotes. However, inhibition of SDF-1α–CXCR4 interactions may be more problematic, because knockout of either the SDF-1α or CXCR4 gene in mice causes severe defects including abnormal hematopoiesis, cerebellar development, and vascularia-

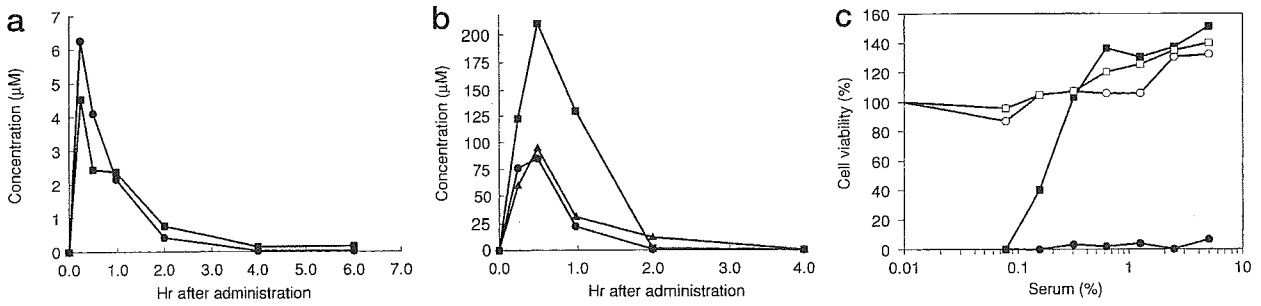

Fig. 3. Absorbability of KRH-1636 and methansulfonated KRH-1636 after intraduodenal administration into Wistar rats. Two and three rats were administered with KRH-1636 (*a*) and methansulfonated KRH-1636 (*b*), respectively. Each symbol represents the data from each animal. (*c*) The MTT assay was carried out by using MT-4 cells to determine the EC_{50} (%) and EC_{90} (%) of serum at 60 min after the administration of KRH-1636. –□–, KRH-1636/mock; –■–, KRH-1636/HIV-1; –○–, control/mock; –●–, control/HIV-1.

tion of the gastrointestinal tract (39–41). Should not the emergence of drug resistance be regarded as a serious matter? It is unlikely that frequent mutations occur in the second ECL of CXCR4. However, HIV-1 may be able to acquire resistance to KRH-1636 by amino acid mutations of the viral envelope protein gp120. In fact, an X4 HIV-1 resistant to SDF-1α and AMD3100 has been reported recently (42). The resistant virus had multiple mutations in gp120 but did not switch chemokine receptor usage. These and related questions will hopefully be answered as coreceptor-based therapies proceed to clinical trials. Acute toxicological studies have indicated the absence of severe toxicity in rats that received KRH-1636 (1.5 mg/kg per day) by i.v. administration for 4 days (data not shown).

In conclusion, KRH-1636, which can be absorbed from the duodenum into the blood, seems to be a promising agent for the treatment and prophylaxis of HIV-1 infection.

This work was supported by grants from the Ministry of Education, Culture, Sports, Science, and Technology of Japan, the Ministry of Health, Labor, and Welfare of Japan, and Core Research for Evolutional Science and Technology of Japan.

1. Gulick, R. M., Mellors, J. W., Havlir, D., Eron, J. J., Gonzalez, C., McMahon, D., Richman, D. D., Valentine, F. T., Jonas, L., Meibohm, A., *et al.* (1997) *N. Engl. J. Med.* **337,** 734–739.
2. Hammer, S. M., Squires, K. E., Hughes, M. D., Grimes, J. M., Demeter, L. M., Currier, J. S., Eron, J. J., Jr., Feinberg, J. E., Balfour, H. H., Jr., Deyton, L. R., *et al.* (1997) *N. Engl. J. Med.* **337,** 725–733.
3. Palella, F. J., Jr., Delaney, K. M., Moorman, A. C., Loveless, M. O., Fuhrer, J., Satten, G. A., Aschman, D. J. & Holmberg, S. D. (1998) *N. Engl. J. Med.* **338,** 853–860.
4. Cameron, D. W., Heath-Chiozzi, M., Danner, S., Cohen, C., Kravcik, S., Maurath, C., Sun, E., Henry, D., Rode, R., Potthoff, A. & Leonard, J. (1998) *Lancet* **351,** 543–549.
5. Feng, Y., Broder, C. C., Kennedy, P. E. & Berger, E. A. (1996) *Science* **272,** 872–877.
6. Deng, H., Liu, R., Ellmeier, W., Choe, S., Unutmaz, D., Burkhart, M., Di Marzio, P., Marmon, S., Sutton, R. E., Hill, C. M., *et al.* (1996) *Nature* **381,** 661–666.
7. Dragic, T., Litwin, V., Allaway, G. P., Martin, S. R., Huang, Y., Nagashima, K. A., Cayanan, C., Maddon, P. J., Koup, R. A., Moore, J. P. & Paxton, W. A. (1996) *Nature* **381,** 667–673.
8. Alkhatib, G., Combadiere, C., Broder, C. C., Feng, Y., Kennedy, P. E., Murphy, P. M. & Berger, E. A. (1996) *Science* **272,** 1955–1958.
9. Bleul, C. C., Farzan, M., Choe, H., Parolin, C., Clark-Lewis, I., Sodroski, J. & Springer, T. A. (1996) *Nature* **382,** 829–833.
10. Oberlin, E., Amara, A., Bachelerie, F., Bessia, C., Virelizier, J. L., Arenzana-Seisdedos, F., Schwartz, O., Heard, J. M., Clark-Lewis, I., Legler, D. F., *et al.* (1996) *Nature* **382,** 833–835.
11. Cocchi, F., DeVico, A. L., Garzino-Demo, A., Arya, S. K., Gallo, R. C. & Lusso, P. (1995) *Science* **270,** 1811–1815.
12. Schols, D., Struyf, S., Van Damme, J., Este, J. A., Henson, G. & De Clercq, E. (1997) *J. Exp. Med.* **186,** 1383–1388.
13. Donzella, G. A., Schols, D., Lin, S. W., Este, J. A., Nagashima, K. A., Maddon, P. J., Allaway, G. P., Sakmar, T. P., Henson, G., De Clercq, E. & Moore, J. P. (1998) *Nat. Med.* **4,** 72–77.
14. Hendrix, C. W., Flexner, C., MacFarland, R. T., Giandomenico, C., Fuchs, E. J., Redpath, E., Bridger, G. & Henson, G. W. (2000) *Antimicrob. Agents Chemother.* **44,** 1667–1673.
15. Masuda, M., Nakashima, H., Ueda, T., Naba, H., Ikoma, R., Otaka, A., Terakawa, Y., Tamamura, H., Ibuka, T., Murakami, T., *et al.* (1992) *Biochem. Biophys. Res. Commun.* **189,** 845–850.
16. Murakami, T., Nakajima, T., Koyanagi, Y., Tachibana, K., Fujii, N., Tamamura, H., Yoshida, N., Waki, M., Matsumoto, A., Yoshie, O., *et al.* (1997) *J. Exp. Med.* **186,** 1389–1393.
17. Baba, M., Nishimura, O., Kanzaki, N., Okamoto, M., Sawada, H., Iizawa, Y., Shiraishi, M., Aramaki, Y., Okonogi, K., Ogawa, Y., *et al.* (1999) *Proc. Natl. Acad. Sci. USA* **96,** 5698–5703.
18. Harada, S., Koyanagi, Y. & Yamamoto, N. (1985) *Virology* **146,** 272–281.
19. Adachi, A., Gendelman, H. E., Koenig, S., Folks, T., Willey, R., Rabson, A. & Martin, M. A. (1986) *J. Virol.* **59,** 284–291.
20. Yoshiyama, H., Kobayashi, N., Matsui, T., Nakashima, H., Kajii, T., Yamato, K., Kotani, S., Miyoshi, I. & Yamamoto, N. (1987) *Mol. Biol. Med.* **4,** 385–396.
21. Yoshiyama, H., Koyanagi, Y., Nakashima, H., Ishihara, T., Uchino, F., Harada, S., Okino, F., Kajii, T. & Yamamoto, N. (1986) *Jpn. J. Cancer Res.* **77,** 16–20.
22. Tanaka, R., Yoshida, A., Murakami, T., Baba, E., Lichtenfeld, J., Omori, T., Kimura, T., Tsurutani, N., Fujii, N., Wang, Z. X., *et al.* (2001) *J. Virol.* **75,** 11534–11543.
23. Inudoh, M., Kato, N. & Tanaka, Y. (1998) *Microbiol. Immunol.* **42,** 875–877.
24. Pauwels, R., Balzarini, J., Baba, M., Snoeck, R., Schols, D., Herdewijn, P., Desmyter, J. & De Clercq, E. (1988) *J. Virol. Methods* **20,** 309–321.
25. Shimizu, N., Naoe, T., Kawazoe, Y., Sakagami, H., Nakashima, H., Murakami, T. & Yamamoto, N. (1993) *Biol. Pharm. Bull.* **16,** 434–436.
26. Chowdhury, I. H., Koyanagi, Y., Kobayashi, S., Hamamoto, Y., Yoshiyama, H., Yoshida, T. & Yamamoto, N. (1990) *Virology* **176,** 126–132.
27. Combadiere, C., Ahuja, S. K. & Murphy, P. M. (1995) *J. Biol. Chem.* **270,** 16491–16494.
28. Power, C. A., Meyer, A., Nemeth, K., Bacon, K. B., Hoogewerf, A. J., Proudfoot, A. E. & Wells, T. N. (1995) *J. Biol. Chem.* **270,** 19495–19500.
29. Raport, C. J., Gosling, J., Schweickart, V. L., Gray, P. W. & Charo, I. F. (1996) *J. Biol. Chem.* **271,** 17161–17166.
30. Holmes, W. E., Lee, J., Kuang, W. J., Rice, G. C. & Wood, W. I. (1991) *Science* **253,** 1278–1280.
31. Tanaka, T., Kitamura, F., Nagasaka, Y., Kuida, K., Suwa, H. & Miyasaka, M. (1993) *J. Exp. Med.* **178,** 1103–1107.
32. Zhu, T., Mo, H., Wang, N., Nam, D. S., Cao, Y., Koup, R. A. & Ho, D. D. (1993) *Science* **261,** 1179–1181.
33. van't Wout, A. B., Kootstra, N. A., Mulder-Kampinga, G. A., Albrecht-van Lent, N., Scherpbier, H. J., Veenstra, J., Boer, K., Coutinho, R. A., Miedema, F. & Schuitemaker, H. (1994) *J. Clin. Invest.* **94,** 2060–2067.
34. Richman, D. D. & Bozzette, S. A. (1994) *J. Infect. Dis.* **169,** 968–974.
35. Mosier, D. E., Gulizia, R. J., Baird, S. M., Wilson, D. B., Spector, D. H. & Spector, S. A. (1991) *Science* **251,** 791–794.
36. Mosier, D. E., Gulizia, R. J., MacIsaac, P. D., Torbett, B. E. & Levy, J. A. (1993) *Science* **260,** 689–692.
37. Suzuki, Y., Koyanagi, Y., Tanaka, Y., Murakami, T., Misawa, N., Maeda, N., Kimura, T., Shida, H., Hoxie, J. A., O'Brien, W. A. & Yamamoto, N. (1999) *J. Virol.* **73,** 316–324.
38. Schols, D. & Verh, K. (1999) *Verh. K. Vlaam. Acad. Geneeskd. Belg.* **61,** 551–564.
39. Nagasawa, T., Hirota, S., Tachibana, K., Takakura, N., Nishikawa, S., Kitamura, Y., Yoshida, N., Kikutani, H. & Kishimoto, T. (1996) *Nature* **382,** 635–638.
40. Tachibana, K., Hirota, S., Iizasa, H., Yoshida, H., Kawabata, K., Kataoka, Y., Kitamura, Y., Matsushima, K., Yoshida, N., Nishikawa, S., *et al.* (1998) *Nature* **393,** 591–594.
41. Zou, Y. R., Kottmann, A. H., Kuroda, M., Taniuchi, I. & Littman, D. R. (1998) *Nature* **393,** 595–599.
42. Schols, D., Este, J. A., Cabrera, C. & De Clercq, E. (1998) *J. Virol.* **72,** 4032–4037.

MOLECULAR REPRODUCTION AND DEVELOPMENT 65:67–72 (2003)

Immunohistochemical Localization of Steroidogenic Enzymes in Human Follicle Following Xenotransplantation of the Human Ovarian Cortex Into NOD-SCID Mice

YUMI SATO,[1] YUKIHIRO TERADA,[1]* HIROKI UTSUNOMIYA,[1] YOSHIO KOYANAGI,[2] MAMORU ITO,[5] ICHIRO MIYOSHI,[3] TAKASHI SUZUKI,[4] HIRONOBU SASANO,[4] TAKASHI MURAKAMI,[1] NOBUO YAEGASHI,[1] AND KUNIHIRO OKAMURA[1]

[1]*Department of Obstetrics and Gynecology, Tohoku University School of Medicine, Seiryo-machi, Aoba-ku, Sendai, Japan*
[2]*Department of Virology, Tohoku University School of Medicine, Seiryo-machi, Aoba-ku, Sendai, Japan*
[3]*Institute for Animal Experimentation, Tohoku University School of Medicine, Seiryo-machi, Aoba-ku, Sendai, Japan*
[4]*Department of Pathology, Tohoku University School of Medicine, Seiryo-machi, Aoba-ku, Sendai, Japan*
[5]*Central Institute for Experimental Animals, Kawasaki, Japan*

ABSTRACT There have been reports of successful follicular growth following xenogenic transplantation of the human ovarian cortex into immunodeficient mice. In this study, we examined the immunohistochemical expression and localization of steroidogenic enzymes in the graft of nonpathological human ovary following xenogenic transplantation into nonobese diabetic severe combined immune deficient (NOD-SCID) mice. We studied human follicles following xenotransplantation into NOD-SCID mice using immunohistochemistry antibodies against the cell proliferation marker (Ki 67), steroidogenic enzymes P450 cholesterol side chain cleavage (P450 scc), 3β-hydroxysteroid dehydrogenase (3β-HSD), cytochrome P450 17α hydroxylase (P450 c17), cytochrome P450 aromatase (P450 arom), androgen receptor (AR), estrogen receptor (ER), and Ad4-binding protein (Ad4BP), a transcription factor for all steroidogenic *P450* genes. In the pre-antral follicles of these grafts, Ki 67 and Ad4BP were detected in both the theca and granulosa cell layer. P450 scc, P450 c17, 3β-HSD, and AR were present in only the theca cell layer, observations of which were consistent with the findings of nonpathological human ovarian cortex. P450 arom and ER were not detected in these grafts, however, and these follicles did not possess any specific feature of a dominant follicle. These findings suggest that the expression of steroidogenic enzymes in human follicles following xenogenic transplantation into NOD-SCID mice is similar to that of nonpathological human ovaries. However, these follicles do not possess any features of dominant follicles, which are known to develop into the corpus luteum. *Mol. Reprod. Dev. 65: 67–72, 2003.* © 2003 Wiley-Liss, Inc.

Key Words: ovarian tissue; xenotransplantation; steroidogenic enzymes; Ad4BP; NOD-SCID mouse

INTRODUCTION

Transplantation of human tissue into experimental animals is used for investigating the process of tissue development. The T and B cell-defect severe combined immune deficient (SCID) mouse has been used as a recipient for the successful transplantation of human tissues (Koyanagi et al., 1997). As an example, human ovarian cortex xenografting into SCID mice is a model for examining the development of the human follicle in ovarian tissues (Oktay et al., 1998, Weissman et al., 1999).

Preservation of human ovarian cortex can be used in the attempt to sustain fertility in disorders that may include irreversible loss of ovarian functions, including ovarian cancer and premature ovarian failure (Kim et al., 2001). The establishment of in vitro oocyte maturation from the human ovarian cortex has not been perfected, despite the improvements of ovarian graft banking.

Several studies have reported the successful reconstitution of human ovarian tissue into immunodeficient mice following transplantation. Weissman et al. (1999) initially described successful subcutaneous transplantation of human ovarian cortex into nonobese diabetic severe combined immune deficient (NOD-SCID) mice. Exogenous gonadotropin stimulation resulted in follicle growth, including the development of antral follicles.

Grant sponsor: Japan Society for the Promotion of Science; Grant sponsor: Kanzawa Medical Research Foundation; Grant sponsor: Gonryo Medical Foundation (to YT).

*Correspondence to: Yukihiro Terada, MD, PhD, Department of Obstetrics and Gynecology, Tohoku University School of Medicine, 1-1 Seiryo-machi, Aoba-ku, Sendai, 980-8574, Japan.
E-mail: terada@ob-gy.med.tohoku.ac.jp

Received 2 September 2002; Accepted 27 November 2002
Published online in Wiley InterScience (www.interscience.wiley.com).
DOI 10.1002/mrd.10260

TABLE 1. Summary of Primary Antibodies Employed in This Study

Antibody	Characteristic	Dilution	Source
P450scc	Polyclonal	×600	Dr. M. Okamoto (Department of Physiological Chemistry, Osaka University Medical Schollo, Osaka, Japan)
3β-HSD	Polyclonal (3β-hsd-P-HU)	×375	Oxygene, Dallas, TX
P450c17	Polyclonal	×250	Dr. J.I. Mason (University of Texas, Southwestern Medical Center, Dallas, TX) (Sasano et al., 1989)
P450arom	Polyclonal	×800	Dr. N. Harada (Fujita-Gakuen Health University, Toyoake, Japan) (Harada, 1988)
AR	Polyclonal	×1,000	A. Mizokami (Department of Molecular and Cell Biology, University of Occupational and Environmental Health, Kitakyushu, Japan) (Kimura et al., 1993)
ER	Monoclonal	×1	Immunotech (ERID5) (Marseilles, France)
Ad4BP	Polyclonal	×500	K. Morohashi (Graduate School of Medical Science, Kyushu University, Fukuoka, Japan) (Morohashi et al., 1993)
Ki 67	Monoclonal	×40	Immunotech (MIB-1) (Marseilles, France)

Furthermore, Gook et al. (2001) reported the development of antral follicles (diameter 0.1–5.0 mm) from human cryopreserved ovarian tissues using this xenotransplantation system. These data suggest that it is possible to collect mature human eggs from these xenografts. A functional assessment of these xenografted ovarian follicles is critical for understanding the mechanisms of steroidogenesis and metabolism in these tissues; however, to date, only morphological studies have been performed.

Investigating the temporal and spatial patterns of steroidogenic enzyme expression in the human ovary is very important for obtaining a better understanding of follicular developmental metabolism. Steroidogenesis in the human ovarian cortex is well known to be regulated by many enzymes, and the localization of these enzymes and related proteins in the premenopausal human ovary has been well documented (Suzuki et al., 1993). Synthesis of these proteins is essential for the process of follicular development. Aberrant expression of these steroidogenic enzymes and sex steroid receptors is frequently detected in some conditions of ovarian dysfunction (Takayama et al., 1996). In addition, the temporal and spatial expression of Ad4-binding protein (Ad4BP), a general regulator of all steroidogenic *P450* genes, has been demonstrated to be involved in the regulation of ovarian steroidogenesis (Takayama et al., 1995).

In the present study, we investigated the expression and localization of steroidogenic enzymes, sex-steroid receptors, and a cell proliferation marker by immunohistochemistry in a human ovarian graft, following xenogenic transplantation into NOD-SCID mice.

MATERIALS AND METHODS

All procedures for collecting human specimens and animal experiments in this study were approved by the Ethics Committee at Tohoku University School of Medicine. (No. 2000-22, No. 2001-297)

Animal Studies

Female NOD-SCID mice were maintained in the Central Institute for Experimental Animals (Kawasaki, Japan) and used at 8–10 weeks of age. The mice were housed in air-filtered isolator. All surgical procedures on the animals were performed in a laminar flow hood.

Human Ovarian Tissue Collection and Transplantation

Ovarian tissue was obtained after receiving informed consent from a woman aged 29 years by biopsy for routine histological evaluation during a gynecological operation. The tissue samples were cut into small cubes (2 × 2 × 2 mm) and immediately placed in warm PBS medium supplemented with 5 IU/L of highly purified human urinary FSH (Fertinorm; Serono Canada, Oakville, Ont., Canada). These pieces were then transplanted into eight recipient mice within 2 hr. Following a small dorsolateral laparotomy, bilateral ovariectomy was performed, and human ovarian tissues were transplanted into the back skin of the NOD-SCID mice under anesthesia, as described previously (Weissman et al., 1999). Some pieces of ovarian tissue were fixed in 4% paraformaldehyde for histological examination. Ten weeks after the transplantation, 5 IU of human menopausal gonadotropin (HMG: Humegon;

Fig. 2. Human ovarian cortex after transplantation into NOD-SCID mice, subsequently followed by human menopausal gonadotropine (HMG) stimulation. **A**: Human early antral follicle developed in NOD-SCID mice 10 weeks after transplantation and subsequently stimulated by a daily intraperitoneal injection of HMG for 14 days (HE staining). **B**: Immunocytochemistry of human early antral follicles using an antibody against Ki 67, in the same early antral follicle as shown in (A). Magnification, ×200; bar = 100 μm.

Fig. 3. Immunocytochemistry of the steroidogenic enzymes in serial sections of a human pre-antral follicle developed in NOD-SCID mice. **A**: Cytochrome P450 17α hydroxylase (P450 c17) staining was localized in the cytoplasm of the theca cells. **B**: 3β-Hydroxysteroid dehydrogenase (3β-HSD) staining localized in the cytoplasm of the theca cells. **C**: Cytochrome P450 aromatase (P450 arom) staining was not observed. **D**: Ad4-binding protein (Ad4BP) was localized in the nuclei of both the theca and granulosa cell layers. **E**: Cytochrome P450 17α hydroxylase staining for nonpathological human ovarian tissue was localized in the cytoplasm of the theca cells, as well as ovarian tissue following transplantation. T: theca cells. G: granulosa cells. Magnification, ×200; bar = 100 μm.

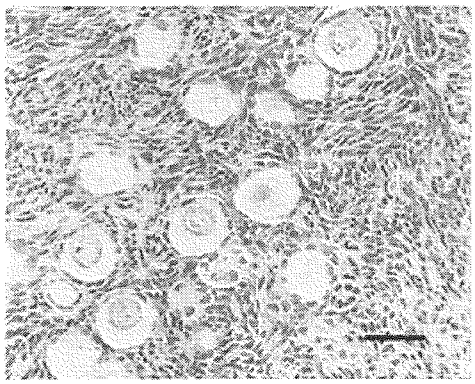

Fig. 1. Human ovarian tissue before transplantation. Only primordial and primary follicles are observed. Hematoxylin and eosin (HE) staining: magnification, ×400; bar = 40 μm.

Organon, Oss, The Netherlands) was intraperitoneally injected daily for 14 days. As controls, two recipient mice were not treated by gonadotropin, and ovarian grafts were collected 12 weeks after the transplantation. All animals were healthy during the entire course of the 12-week experiment.

Immunohistochemical Analysis of Ovarian Tissue

The characteristics of the primary antibodies employed in this study are summarized in Table 1.

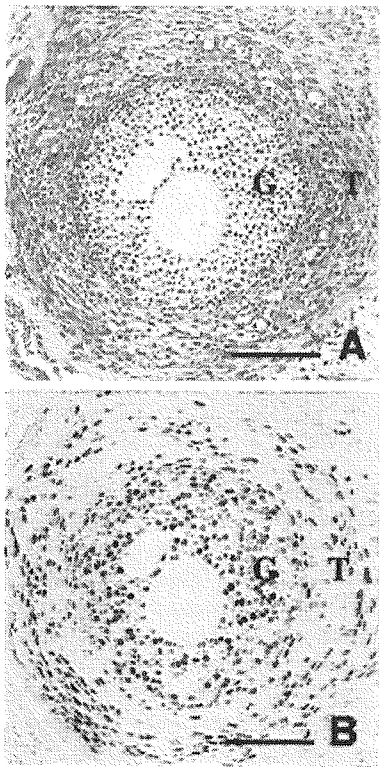

Fig. 2.

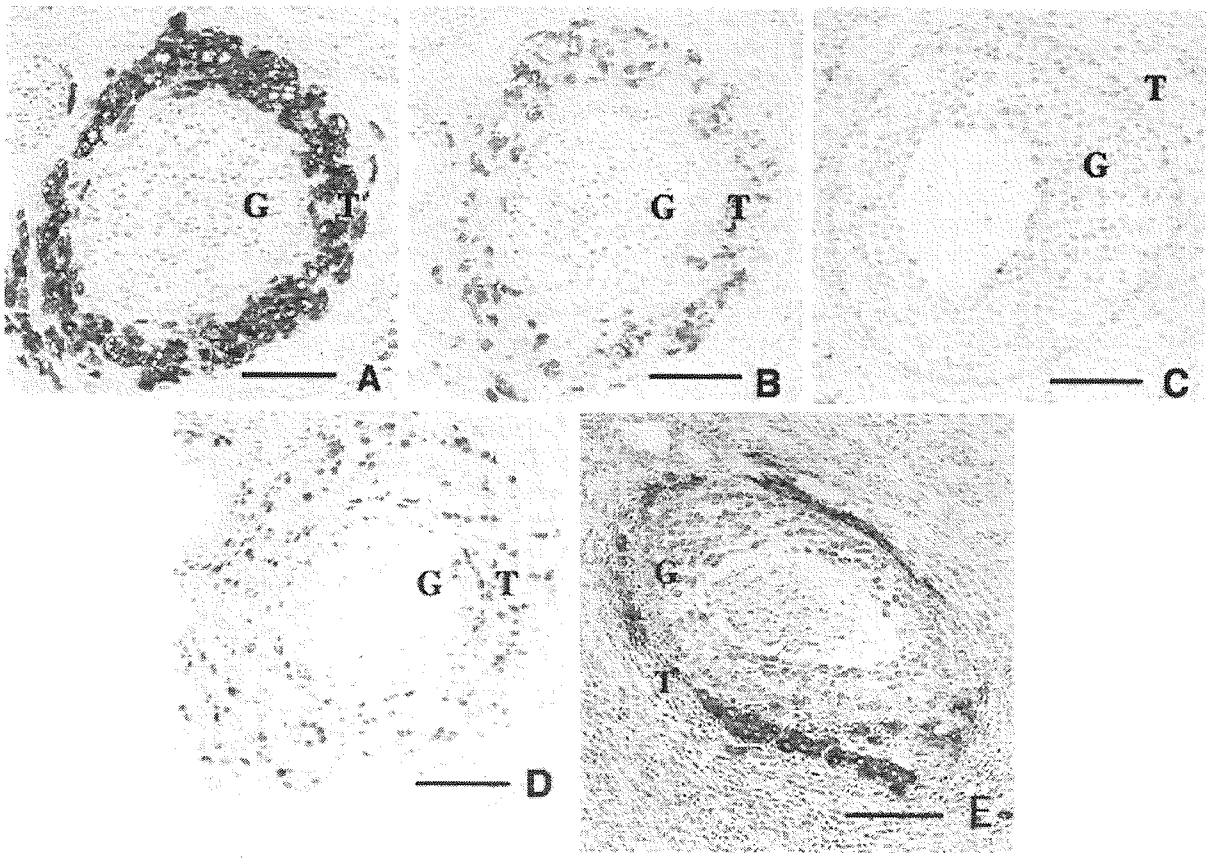

Fig. 3.

TABLE 2. Immunohistochemical Localization of P450scc, 3β-HSD, P450c17, P450arom, ER, AR, Ad4BP and Ki 67 Expression in Xenografting Human Follicles

		Steroidogenic enzymes				Receptors			
Follicle stages	Cell type	P450scc	3β-HSD	P450c17	P450arom	AR	ER	Ad4BP	Ki 67
Primordial	G	–	–	–	–	–	–	–	–
	S	–	–	–	–	–	–	–	–
Primary	G	–	–	–	–	–	–	–	–
	S	–	–	–	–	–	–	–	–
Preantral	G	–	–	–	–	–	–	–	–
	T	–	–	–	–	–	–	–	–
Early antral	G	–	–	–	–	–	–	+	++
	T	++	++	++	–	++	–	+	++

NOD-SCID mice were euthanized 12 weeks after the transplantation. Human ovarian grafts were retrieved and fixed in 4% paraformaldehyde, cut into 3-μm-thick sections and mounted on poly-L-lysine-coated glass slides (Matsunami, Tokyo, Japan). Immunohistochemical analyses were performed employing the streptavidin–biotin amplification method in a Histofine Kit (Nichirei, Tokyo, Japan), as previously described (Suzuki et al., 1993; Takayama et al., 1995). The antigen-antibody complex was visualized with 3.3-diaminobenzidine (DAB) solution {1 mM DAB, 50 mM Tris-HCl buffer (pH 7.6), and 0.006% H_2O_2} and counterstained with hematoxylin. Staining for androgen receptor (AR), estrogen receptor (ER), Ad4BP, and Ki 67 was performed by placing sections in citric acid buffer (2 mM citric acid, 9 mM trisodium citrate dihydrate, pH 6.0), and heating the solution in an autoclave for 5 min for antigen retrieval. Tissue sections of full-term placenta were used as positive controls for P450 cholesterol side chain cleavage (P450 scc), P450 17α hydroxylase (P450 c17), 3β-hydroxysteroid dehydrogenase (3β-HSD) (Sasano et al., 1989), and P450 aromatase (P450arom) (Harada, 1988; Sasano et al., 1996; Suzuki et al., 1998). As a control, P450 c17 immunoreactivity for nonpathological human ovarian tissue was examined, as well as above method. For the evaluation of immunoreactivity, we employed a labeling index (LI: i.e., the percentage of positive cells) according to a report by Sasano et al. (1989). After completely reviewing the immunostained sections of each lesion, two of the authors (YS and HU) independently divided the cases into the following three groups: ++, more than 50% positive cells; +, 1–50% positive cells; and –, no immunoreactivity. Scoring of Ki 67, P450 scc, P450 c17, 3β-HSD, P450 arom, AR, ER, and Ad4BP in granulosa and theca cells was performed on high power fields (× 200) using a standard light microscope. A total of more than 500 granulosa and theca cells were counted independently by the same two authors, and the percentage of immunoreactivity (i.e., the LI) was determined. Cases with disconcordant results (interobserver differences of more than 5%) were simultaneously re-evaluated by the same two authors using double-headed light microscopy. Consequently, interobserver differences were less than 5% in this study.

RESULTS

Follicle Survival and Development in Human Xenografts

Ovarian follicles were classified based on the criteria of Clement (1987). We noted the absence of any follicle more advanced than the primary stage in ovarian tissues before transplantation (Fig. 1). Twelve weeks after transplantation, only primary or secondary follicles were observed, in the grafts without gonadotropine stimulation whereas the development of follicles at all stages including the early antral stage was observed in the ovarian graft after transplantation and gonadotropine stimulation.

Expression and Localization of Cell Proliferating Marker, Steroidogenetic Enzymes, and Ad4BP in Xenografts

The expression and localization of cell proliferating marker, steroidogenic enzymes, Ad4BP, AR, and ER in xenografts are summarized in Table 2. In early antral follicles, immunoreactivity of the cell proliferating marker Ki 67 was observed in both the granulosa cell and theca cell layers (Fig. 2). The steroidogenic enzymes P450 scc, P450 c17 (Fig. 3A), and 3β-HSD (Fig. 3B) were observed in the cytoplasm of the theca cells. However, P450 arom and ER expression was negative in cells of early antral follicles (Fig. 3C). Ad4BP staining was observed in the nuclei of both the theca and granulosa cell layer (Fig. 3D). AR expression was also observed in the nuclei of theca cells.

DISCUSSION

Xenografting of human ovarian tissue into an animal host followed by subsequent follicular development has been proposed as a method to preserve the fertility of cancer survivors. Furthermore, there are numerous unsolved difficulties with respect to the in vitro culturing of human primordial follicles that an in vivo system can overcome (Liu et al., 2000; Van den Broecke et al., 2001). Several studies have reported that antral follicles appear to develop in a graft from both normal and cryopreserved ovarian tissues (Oktay et al., 1998). However, to date, trials have only involved the morphological assessment of follicular development.

Follicular development in the ovarian cortex is promoted by a number of autocrine and paracrine endocrine systems (Morohashi et al., 1993; Callejo et al., 1999). The temporal and spatial expression and localization of steroidogenic enzymes in the human premenopausal cycling ovary has been examined by Sasano et al. (1996). P450 scc, which catalyzes the conversion of cholesterol to pregnenolone; 3β-HSD, which catalyzes the conversion of pregnenolone to progesterone; and P450 c17, which catalyses the conversion of progesterone to androstenedione, have been shown to be sporadically expressed in the theca cells of relatively large-sized pre-antral follicles (Suzuki et al., 1993). AR was also detected in the theca cell layer, whereas ER was positive only in the P450 arom-positive antral or preovulatory follicle (Suzuki et al., 1998; Vendola et al., 1998; Saunders et al., 2000). A family of steroidogenic enzymes, in particular P450 (scc, c17, arom), is critical, and Ad4BP, a transcription factor that regulates many of the steroidogenic *P450* genes, must be recruited in both the granulosa and theca layer of the dominant follicle. In contrast, within the same nondominant antral follicle, Ad4BP was absent, suggesting that this was a key factor for ovarian steroidogenesis (Honda et al., 1993; Takayama et al., 1995). Furthermore, it has been demonstrated that the expression of Ki 67 is significantly augmented in both the theca and granulosa layer of antral follicles but not in primary and/or primordial follicles (Funayama et al., 1996).

In this study, we examined the expression and localization of Ki 67, steroidogenic enzymes, AR, ER, and Ad4BP in human follicles obtained after xenografting. Immunoreactive Ki 67 was observed in both the theca and granulosa cell layers, suggesting that the ovarian grafts investigated in our study were actively involved in the cell proliferation phase, as observed in the early antral follicle of nonpathological human ovaries. Immunoreactive proteins for P450 scc, 3β-HSD, and P450 c17 were localized only in the theca cell layer, whereas Ad4BP was observed in both the granulosa and theca cell layers. P450 c17 immunoreactivity for nonpathological human ovarian tissue was expressed in the cytoplasm of the theca cell layer, as well as ovarian tissue following transplantation (Fig. 3E). In addition, AR was found to be expressed in the theca cell layer. The immunoreactive localization of these peptides strikingly resembles that of nonselected antral follicles in the nonpathological human ovary (Suzuki et al., 1998). However, neither ER nor P450 arom was found in any of the theca cells examined. These follicles still do not complete estrogen synthesis, a final goal of selected and matured human follicles. The expression of P450 arom was generally observed in only one follicle (antral or preovulatory) in the human ovary, according to Suzuki et al. (1993).

Estrogen plays roles in folliculogenesis via an autocrine system and is also required for the completion of oocyte cytoplasmic maturation (Tesarik and Mendoza, 1995). Further studies are needed to assess the developmental potential of oocytes from this xenografting system, in which follicles lack the characteristics of dominant follicles.

The mechanism involved in the recruitment of primordial follicles into the antral follicle stage is unknown, and this model system has the potential to elucidate follicle developmental mechanisms. Furthermore, elucidation of follicular development in this immuno-compromised heterologous system would contribute to the establishment of an in vitro system to obtain matured oocytes from the human ovarian cortex. This system can be used not only in ovarian banking but also as a model to delineate the mechanism of folliculogenesis.

REFERENCES

Callejo J, Jauregui MT, Valls C, Fernandez ME, Cabre S, Lailla JM. 1999. Heterotopic ovarian transplantation without vascular pedicle insyngeneic Lewis rats: Six-month control of estradiol and follicle-stimulating hormone concentrations after intraperitoneal and subcutaneous implants. Fertil Steril 72:513–517.

Clement PB. 1987. Histology of the ovary. Am J Surg Pathol 11:277–303.

Funayama Y, Sasano H, Suzuki T, Tamura M, Fukaya T, Yajima A. 1996. Cell turnover in normal cycling human ovary. J Clin Endocrinol Metab 81:828–834.

Gook DA, McCully BA, Edgar DH, McBain JC. 2001. Development of antral follicles in human cryopreserved ovarian tissue following xenografting. Human Reprod 16:417–422.

Harada N. 1988. Novel properties of human placental aromatase as cytochrome P-450: Purification and characeterization of a unique form of aromatase. J Biochem Tokyo 103:106–113.

Honda S, Morohashi K, Nomura M, Takeya H, Kitajima M, Omura T. 1993. Ad4BP regulating steroidogenic *P-450* gene is a member of steroid hormone receptor superfamily. J Biol Chem 268: 7494–7502.

Kim SS, Battaglia DE, Soules MR. 2001. The future of human ovarian cryopreservation and transplantation: Fertility and beyond. Fertil Steril 75:1049–1056.

Kimura N, Mizokami A, Oonuma T, Sasano H, Nagura H. 1993. Immunohistochemical localization of androgen receptor with polyclonal antibody in paraffin-embedded human tissues. J Histochem Cytochem 41:671–678.

Koyanagi Y, Tanaka Y, Kira J, Ito M, Hioki K, Misawa N, Kawano Y, Yamasaki K, Tanaka R, Suzuki Y. 1997. Primary human immunodeficiency virus type 1 viremia and central nervous system invasion in a novel hu-PBL-immunodeficient mouse strain. J Virol 71:2417–2424.

Liu J, Van der Elst J, Van den Broecke R, Dumortier F, Dhont M. 2000. Maturation of mouse primordial follicles by combination of grafting and in vitro culture. Biol Reprod 62:1218–1223.

Morohashi K, Zanger UM, Honda S, Hara M, Waterman MR, Omura T. 1993. Activation of CYP11A and CYP11B gene promoters by the steroidogenic cell-specific transcription factor, Ad4BP. Mol Endocrinol 7:1196–1204.

Oktay K, Newton H, Mullan J, Gosden RG. 1998. Development of human primordial follicles to antral stages in SCID/hpg mice stimulated with follicle stimulating hormone. Hum Reprod 13:1133–1138.

Sasano H, Okamoto M, Mason JI, Simpson ER, Mendelson CR, Sasano N, Silverberg SG. 1989. Immunolocalization of aromatase, 17α-hydroxylase and side-chain-cleavage cytochromes P-450 in the human ovary. J Reprod Fertil 85:163–169.

Sasano H, Frost AR, Saitoh R, Harada N, Poutanen M, Vihko R, Bulun SE, Silverberg SG, Nagura H. 1996. Aromatase and 17β-hydrozysteroid dehydrogenase type 1 in human brest carcinoma. J Clin Endocrinol Metab 81:4042–4046.

Saunders PT, Millar MR, Williams K, Macpherson S, Harkiss D, Anderson RA, Orr B, Groome NP, Scobie G, Fraser HM. 2000. Differential expression of estrogen receptor-alpha and -beta and

androgen receptor in the ovaries of marmosets and humans. Biol Reprod 63:1098–1105.

Suzuki T, Sasano H, Tamura M, Aoki H, Fukaya T, Yajima A, Nagura H, Mason JI. 1993. Temporal and spatial localization of steroidogenic enzymes in premenopausal human ovaries: In situ hybridization and immunohistochemical study. Mol Cell Endocrinol 97:135–143.

Suzuki T, Sasano H, Kimura N, Tamura M, Fukaya T, Yajima A, Nagura H. 1998. Immunohistochemical distribution of progesterone, androgen, and oestrogen receptors in the human ovary steroidogenic enzymes. Hum Reprod 13:1922–1927.

Takayama K, Sasano H, Fukaya T, Morohashi K, Suzuki T, Tamura M, Costa MJ, Yajima A. 1995. Immunohistochemical localization of Ad4-binding protein with correlation to steroidogenic enzyme expression in cycling human ovaries and sex cord stromal tumors. J Clin Endocrinol Metab 80:2815–2821.

Takayama K, Fukaya T, Sasano H, Funayama Y, Suzuki T, Takaya R, Wada Y, Yajima A. 1996. Immunohistochemical study of steroidogenesis and cell proliferation in polycystic ovarian syndrome. Human Reprod 11:1387–1392.

Tesarik J, Mendoza C. 1995. Nongenomic effects of 17 beta-estradiol on maturing human oocytes: Relationship to oocyte developmental potential. J Clin Endocrinol Metab 80:1438–1443.

Van den Broecke R, Liu J, Handyside A, Van der Elst JC, Krausz T, Dhont M, Winston RM, Hovatta O. 2001. Follicular growth in fresh and cryopreserved human ovarian cortical grafts transplanted to immunodeficient mice. Eur J Obstet Gynecol Reprod Biol 97: 193–201.

Vendola KA, Zhou J, Adesanya OO, Weil SJ, Bondy CA. 1998. Androgens stimulate early stages of follicular growth in the primate ovary. J Clin Invest 15:2622–2629.

Weissman A, Gotlieb L, Colgan T, Jurisicova A, Greenblatt EM, Casper RF. 1999. Preliminary experience with subcutaneous human ovarian cortex transplantation in the NOD-SCID mouse. Biol Reprod 60: 1462–1467.

JOURNAL OF VIROLOGY, May 2003, p. 5286–5294 Vol. 77, No. 9
0022-538X/03/$08.00+0 DOI: 10.1128/JVI.77.9.5286–5294.2003

Rapid Tumor Formation of Human T-Cell Leukemia Virus Type 1-Infected Cell Lines in Novel NOD-SCID/γc^{null} Mice: Suppression by an Inhibitor against NF-κB

M. Zahidunnabi Dewan,[1] Kazuo Terashima,[1] Midori Taruishi,[1] Hideki Hasegawa,[2] Mamoru Ito,[3] Yuetsu Tanaka,[4] Naoki Mori,[5] Tetsutaro Sata,[2] Yoshio Koyanagi,[6] Michiyuki Maeda,[7] Yoko Kubuki,[8] Akihiko Okayama,[8] Masahiro Fujii,[9] and Naoki Yamamoto[1]*

Department of Molecular Virology, Bio-Response, Graduate School, Tokyo Medical and Dental University, Tokyo 113-8519,[1] Department of Pathology, National Institute of Infectious Diseases, Tokyo 162-8640,[2] Central Institute for Experimental Animals, Kawasaki 216,[3] Department of Infectious Disease and Immunology, Okinawa-Asia Research Center of Medical Science,[4] and Department of Virology,[5] Faculty of Medicine, University of the Ryukyus, Okinawa 905-0215, Department of Virology, School of Medicine, Tohoku University, Sendai 980-8575,[6] Institute for Frontier Medical Sciences, Kyoto University, Kyoto 606-8507,[7] Department of Internal Medicine II, Miyazaki Medical College, Miyazaki 889-1601,[8] and Department of Virology, Niigata University School of Medicine, Niigata 951,[9] Japan

Received 16 August 2002/Accepted 24 January 2003

We established a novel experimental model for human T-cell leukemia virus type 1 (HTLV-1)-induced tumor using NOD-SCID/γc^{null} (NOG) mice. This model is very useful for investigating the mechanism of tumorigenesis and malignant cell growth of adult T-cell leukemia (ATL)/lymphoma, which still remains unclear. Nine HTLV-1-infected cell lines were inoculated subcutaneously in the postauricular region of NOG mice. As early as 2 to 3 weeks after inoculation, seven cell lines produced a visible tumor while two transformed cell lines failed to do so. Five of seven lines produced a progressively growing large tumor with leukemic infiltration of the cells in various organs that eventually killed the animals. Leukemic cell lines formed soft tumors, whereas some transformed cell lines developed into hemorrhagic hard tumors in NOG mice. One of the leukemic cell lines, ED-40515(−), was unable to produce visible tumors in NOD-SCID mice with a common γ-chain after 2 weeks. In vivo NF-κB DNA binding activity of the ED-40515(−) cell line was higher and the NF-κB components were changed compared to cells in vitro. Bay 11-7082, a specific and effective NF-κB inhibitor, prevented tumor growth at the sites of the primary region and leukemic infiltration in various organs of NOG mice. This in vivo model of ATL could provide a novel system for use in clarifying the mechanism of growth of HTLV-1-infected cells as well as for the development of new drugs against ATL.

Human T-cell leukemia virus type-1 (HTLV-1) induces adult T-cell leukemia/lymphoma (ATL/L), a fatal lymphoproliferative disorder, and HTLV-1-associated myelopathy/tropical spastic paraparesis, a chronic progressive disease of the central nervous system after a long period of latent infection (12, 33, 48). This long latency suggests that multiple genetic events, which accumulate in HTLV-1-infected cells, are involved in the development of ATL. HTLV-1 transforms primary human T-cells in vitro and a unique viral gene Tax is considered to play a central role in HTLV-1-induced transformation. However, HTLV-1-infected cell lines derived from a leukemic cell clone failed to express significant amounts of Tax and other viral proteins, suggesting that the expression of viral proteins is not always necessary for leukemic proliferation at the late stage of the disease. On the other hand, the observation that NF-κB, which is strongly induced by Tax, is indispensable for the maintenance of the malignant phenotype of HTLV-1 provides a possible molecular target for ATL therapy (23, 39) as well as the treatment of some cancers (1, 14, 40). In resting cells, binding to inhibitory IκBs retains NF-κB in the cytoplasm in an inactive form. On stimulation, IκBs are rapidly phosphorylated, ubiquitinated, and degraded by a proteosome-dependent pathway allowing active NF-κB to translocate into the nucleus where it can activate the expression of a number of genes (2). Like HTLV-1-infected cells in vitro, leukemic cells from ATL patients in vivo display a constitutive NF-κB binding activity and increased degradation of IκBα (28). However, the precise molecular mechanism of tumorigenesis and the development of ATL after HTLV-1 infection remain obscure.

The severe combined immunodeficient (SCID) mice lacking functional T and B cells (4, 27) were engrafted successfully with human hematopoietic or neoplastic cells (6, 13, 17, 20, 21, 30, 34, 35, 44). SCID mice also have been utilized in a study on the mechanism and therapeutic strategy of ATL. Indeed, it has been reported that HTLV-1-infected cell lines derived from a leukemic clone produced tumors during a 2- to 4-month follow-up period but in vitro-transformed cell lines expressing Tax and other viral antigens failed to do so in SCID mice even at 6 months after inoculation (10, 16). However, two major drawbacks, namely, the long period of time required for tumor formation and the limitation of its use to certain cell lines, appear to hinder wider use of this animal model. To overcome

* Corresponding author. Mailing address: Department of Molecular Virology, Bio-Response, Graduate School, Tokyo Medical and Dental University, 1-5-45 Yushima, Bunkyo-ku, Tokyo 113-8519, Japan. Phone: 81-3-5803-5178. Fax: 81-3-5803-0124. E-mail: yamamoto.mmb@tmd.ac.jp.

these problems we have developed a new SCID mouse strain, the NOG mouse, which is a special type of animal that has immunological multifunctional defects in NK activity, macrophage function, complement activity and function of dendritic cells (18). HTLV-1-infected cell lines were inoculated subcutaneously in the postauricular region of NOG mice enabling macroscopic observation in the study of the mechanism of tumorigenesis and malignant growth of ATL and the development of new drugs against ATL.

There is no effective treatment for ATL patients. ATL still has a poor prognosis mainly because of its resistance to conventional as well as high-dose chemotherapy. Bay 11-7082 is a selective inhibitor of tumor necrosis factor alpha-induced phosphorylation of IκBα without affecting the constitutive activation of IκBα phosphorylation, resulting in decreased NF-κB and decreased expression of adhesion molecules (31). Very recently, we reported that Bay 11-7082 specifically inhibited nuclear translocation of NF-κB and caused selective apoptosis of HTLV-1-infected cell lines and primary ATL cells in vitro (29). In addition, this compound is also known to induce apoptosis of lymphoma cells from patients with primary effusion lymphoma or cutaneous T-cell lymphoma in vitro (19, 22).

We show here that a progressively growing large tumor was rapidly and reproducibly induced in mice inoculated with HTLV-1-infected cell lines derived from both leukemic and transformed cell clones only within 2 weeks. We also examined in vivo tumor growth of an HTLV-1-infected cell line between NOG and NOD-SCID mice to address the role of the common γ-chain. We also provide evidence that the NF-κB-inhibitory effect of Bay 11-7082 is linked to regression of the tumor and that the drug prevented leukemic infiltration of tumor cells in various organs of NOG mice. These results suggest that the NOG mouse model of HTLV-1-infected cell lines would be useful for investigating the in vivo molecular pathogenesis of diseases, infiltration into different organs and therapeutic measures for ATL patients.

MATERIALS AND METHODS

Mice. NOG and NOD-SCID mice were obtained from the Central Institute for Experimental Animals (Kawasaki, Japan). All mice were bred and maintained under specific-pathogen-free conditions in the Animal Center of National Institute of Infectious Diseases (Tokyo, Japan). The Ethical Review Committee of the Institute approved the experimental protocol.

Cell lines. ED-40515(−), MT-1, and TL-Oml are interleukin-2 (IL-2)-independent and Tax nonexpressing human T-cell lines of leukemic cell origin established from ATL patients. SLB-1, Hut-102, MT-2, MT-4, M8116, and TY8-3/MT-2 are IL-2-independent and Tax expressing HTLV-1-infected transformed T-cell lines, and Jurkat is an HTLV-1-negative T-cell line. These cell lines were cultured in RPMI 1640 medium (Nikken Bio-laboratory, Kyoto, Japan) with 10% heat-inactivated fetal bovine serum (JRH Biosciences, Lenexa, Kans.), 2 mM L-glutamine, 100 U of penicillin per ml, and 100 μg of streptomycin per ml at 37°C and 5% CO_2.

Inoculation of cell lines into SCID mice. Cells were washed twice with serum-free RPMI 1640 medium. These cells were resuspended in serum-free RPMI 1640 medium. Mice were anesthetized with ether and cells were inoculated subcutaneously in the postauricular region of SCID mice at a dose of 1 to 7.5 × 10^7 cells per mouse.

Growth measurement of subcutaneous tumor and dispersion of cells. Mice were sacrificed during the 2- to 3-week follow-up period after inoculation with different cell lines. The subcutaneous tumor was excised from the postauricular region of SCID mice. We measured the length, width, and height of the tumor by the Somers scale. Tumor tissues obtained from mice inoculated with the ED-40515(−) cell line after 1 week and 2 weeks for measuring the growth curve in both strains of mice. Next, the tumor tissues were incubated and digested by shaking in RPMI 1640 plus 10% fetal calf serum containing collagenase (1 mg/ml; Seikagaku Kogyo, Tokyo, Japan) plus DNase type I (0.5 mg/ml; Sigma) at 37°C for 30 min. Dispersed cells were collected and the same procedure was conducted as described above. All dispersed cells were filtered with a 40-μm-pore-size filter and washed twice with serum-free medium at 400 × *g* for 5 min. The supernatant was aspirated and the cell pellets were collected. Number of cells was counted by the trypan blue method.

Histological and cytological examination. After sacrificing the mice, tumor tissues, peripheral blood, and various organs were collected. Part of the excised tumor tissues were fixed with dry-ice acetone and embedded in Tissue-Tek OCT compound (Sakura Finetechnical Co. Ltd., Tokyo, Japan) and stored at −80°C before use. Frozen sections of the tumor tissues were prepared by Cryostat and fixed in acetone at room temperature for 20 min. The remaining tumor tissues and organs were fixed with 4% paraformaldehyde for hematoxylin and eosin (H&E) staining and examined under a microscope. Blood was collected from the heart of mice with heparinized syringes. Peripheral blood mononuclear cells (PBMNCs) were isolated from the blood by density gradient concentration with Ficoll-Hypaque. Cytospin specimens of in vitro culture cells and PBMNCs were prepared and fixed in methyl alcohol for May-Grunwald and Giemsa staining and fixed in acetone for immunostaining. For immunostaining, frozen sections of tumor tissues and cytospin samples of in vitro culture cells were incubated with a 1:50 dilution of primary antibody against human cells, anti-CD4 (Novocastra Laboratory. Ltd.), anti-CD25 (Kamiya Biomedical Company, Seattle, Wash.), anti-CD3, and anti-CD8 mouse (DAKO A/S), anti-Tax (MI-73) and anti-Gag (GIN-14) mouse monoclonal antibodies. This was followed by washing in phosphate-buffered saline (PBS) and then incubation with horseradish peroxidase-conjugated rabbit anti-mouse immunoglobulin G antibody (1:200) and washed in PBS. Positive staining was visualized after incubation of these samples with a mixture of 0.05% 3,3′-diaminobenzidine tetrahydrochloride in 50 mM Tris-HCl buffer and 0.01% hydrogen peroxide for 5 to 10 min. The samples were counterstained with methyl green for 15 min, hydrated completely, cleaned in xylene, and then mounted.

Western blotting. Culture cells and cells from tumors were lysed by a low-salt lysis buffer (10 mM Tris-HCl [pH 8.0], 140 mM NaCl, 3 mM $MgCl_2$, 1 mM phenylmethylsulfonyl fluoride [PMSF], and 0.5% Nonidet) on ice for 30 min, followed by centrifugation at 14,000 rpm for 10 min at 4°C. The cell lysates were mixed with an equal volume of twofold-concentrated sample buffer with 2-mercaptoethanol and treated for 5 min at 100°C. Equal amounts (25 μg) of protein from the cell lysates were electrophoresed on sodium dodecyl sulfate–10% polyacrylamide gel and transferred to a Clear Blot Membrane-p (ATTO, Tokyo, Japan) by an electric Western blotting system. The membranes were washed with PBS-Tween (0.1%) and blocked in PBS containing 3% skim milk overnight at 4°C. The membranes were incubated with 1 μg per ml of primary antibody, anti-Tax monoclonal antibody (MI-73) followed by washing in PBS-Tween (0.1%) and incubated again with horseradish peroxidase-conjugated rabbit anti-mouse immunoglobulin G (1:3,000). Protein bands were visualized by an enhanced chemiluminescence substrate and the FLA-2000 system (Fuji Photo Film Co. Tokyo, Japan).

Preparation of nuclear extracts. Cells (3 × 10^6) were washed twice with cold PBS and the cell pellet was resuspended in 200 μl of hypotonic buffer A (HEPES, 10 mmol/liter, pH 7.9; KCl, 10 mmol/liter; EDTA, 0.15 mmol/liter; EGTA, 0.15 mmol/liter; PMSF, 0.1 mmol/liter; leupeptin, 100 μg/liter; aprotinin, 100 μg/liter) including 1% Nonidet and incubated on ice for 15 min. Cell suspensions were vortexed briefly and microcentrifuged at 14,000 rpm for 5 min at 4°C. The supernatants were removed, and the cell pellets were suspended in 200 μl of isotonic B buffer (HEPES, 20 mmol/liter, pH 7.8; NaCl, 100 mmol/liter; EDTA, 0.1 mmol/liter; 25% glycerol), vortexed briefly and microcentrifuged at 14,000 rpm for 3 min at 4°C. Thereafter, the cell pellets were resuspended in 100 μl of hypertonic C buffer (HEPES, 20 mmol/liter, pH 7.8; NaCl, 400 mmol/liter; EDTA, 0.1 mmol/liter; 25% glycerol; PMSF, 0.1 mmol/liter; leupeptin, 100 μg/liter; aprotinin, 100 μg/liter; DTT, 10 mmol/liter) including 1 M NaCl, inoculated at 4°C for 30 min with continuous high speed shaking and microcentrifuged at 14,000 rpm for 3 min. The supernatants were collected, the protein concentrations measured by the method of Bradford and the supernatants stored at −80°C for use.

Electrophoresis mobility shift assay (EMSA). As previously described, nuclear extracts (5 μg of protein) were incubated in 12 μl of binding buffer (HEPES, 10 mmol/liter, pH 7.8; NaCl, 100 mmol/liter; EDTA 1 mmol/liter; 25% glycerol), 1 μg of poly [d(I-C)] and ^{32}P-labeled κB probe derived from the H-2K promoter (22a) for 30 min at room temperature. To identify the subunits constituting the NF-κB complexes, specific antibodies against p50, p65, and c-Rel (Santa Cruz Biotechnology, Santa Cruz, Calif.) were used. Antibodies was added to the nuclear extract, and the mixture was allowed to stand for 30 min at room

TABLE 1. In vitro and in vivo characteristics of HTLV-1-infected cell lines

Cell line	Origin[a]	In vitro characteristics		No. of cells inoculated/mouse (10^7)[c]	In vivo characteristics			
		Proliferation pattern	Tax[b]		Inoculation route[d]	No. of mice with visible tumor/no. of mice inoculated[e]	Day of sacrifice	Average size of tumor (mm)[f]
ED-40515(−)	L	Dispersed	−	1	s.c.	37/37	15	25 × 20 × 12
				7.5	i.m.	1/1	15	23 × 18 × 12
SLB-1	IT	Clustered	+	1	s.c.	15/15	15	19 × 10 × 16
				7.5	i.m.	1/1	15	20 × 10 × 15
MT-1	L	Dispersed	−	1	s.c.	7/7	22	22 × 15 × 10
				7.5	i.m.	1/1	20	21 × 14 × 10
TL-oml	L	Dispersed	−	1	s.c.	7/7	22	23 × 15 × 10
				7.5	i.m.	1/1	20	18 × 15 × 10
Hut-102	IT	Clustered	+	1	s.c.	4/4	22	21 × 13 × 16
				7.5	i.m.	1/1	20	10 × 10 × 7
MT-2	IT	Clustered	+	7.5	s.c.	1/1	20	10 × 9 × 8
				7.5	i.m.	1/1	20	9 × 10 × 7
MT-4	IT	Clustered	+	7.5	s.c.	1/1	20	5 × 5 × 4
				7.5	i.m.	1/1	20	5 × 4 × 3
M8116	IT	Clustered	+	7.5	s.c.	0/1	20	Sesame
				7.5	i.m.	0/1	20	Sesame
TY8-3/MT-2	IT	Clustered	+	7.5	s.c.	0/1	20	Sesame
				7.5	i.m.	0/1	20	Sesame

[a] L, leukemic; IT, in vitro transformed.
[b] −, negative; +, positive.
[c] Mice were injected with 1×10^7 to 7.5×10^7 cells per mouse.
[d] s.c., subcutaneous; i.m., intramuscular.
[e] Number of animals in which visible tumor developed.
[f] Average tumor size of individual mouse was measured as described in Materials and Methods and is given here as length × width × height.

temperature before incubation with the radiolabeled probe. DNA-protein complexes were analyzed by electrophoresis in 5% polyacrylamide gel in 0.5× TBE (Tris, 44.5 mmol/liter; boric acid, 44.5 mmol/liter; EDTA, 1 mmol/liter). After electrophoresis, the gels were dried and subjected to autoradiography.

Administration of Bay 11-7082. Bay 11-7082 was obtained from the Calbiochem-Novabiochem Corporation, La Jolla, Calif. The drug was administered intraperitoneally to mice at doses of 20 mg/kg/day, beginning on day 0 for 20 days. The control mice received 1% dimethyl sulfoxide (DMSO) simultaneously with HTLV-1-infected cells. In other experiments, Bay 11-7082 or DMSO was also administered into the tumor site directly everyday for 15 days at the same doses as stated above 10 days after tumor formation.

RESULTS

Rapid growth of HTLV-1-infected cell lines inoculated in NOG mice. To investigate the in vivo growth, cells of nine IL-2-independent HTLV-1-infected cell lines were inoculated subcutaneously in the postauricular region of NOG mice (Table 1). Mice inoculated with seven cell lines [ED-40515(−), SLB-1, MT-1, TL-Oml, Hut-120, MT-2, and MT-4] produced a visible tumor within 2 to 3 weeks in NOG mice (Fig. 1). The remaining two transformed cell lines (M8116 and TY8-3/MT-2) failed to form a visible tumor during the 2- to 3-week follow-up period although the mice inoculated with these cell lines were found to have sesame-like tumors at the inoculated site after excision of skin. Histological analysis revealed that the sesame-like tumors consist of small number of nonmitotic cells scattering in the scar tissue. Furthermore, no leukemic infiltration was found in various organs of mice with sesame-like tumors (Table 2). Five cell lines [ED-40515(−), SLB-1, Hut-102, MT-1, and TL-Oml] produced a progressively growing large tumor. Especially, ED-40515(−) leukemic and SLB-1 transformed cell lines were most efficient resulting in the formation of a large tumor in NOG mice only after 2 weeks. It was notable that SLB-1- and Hut-102-transformed cell lines produced a hemorrhagic hard tumor and ED-40515(−), MT-1, and TL-Oml leukemic cell lines produced a soft tumor in NOG mice. The average tumor size in NOG mice inoculated with ED-40515(−) and SLB-1 was 25 by 20 by 12 mm and 19 by 10 by 16 mm, respectively, 2 weeks after inoculation. These results showed that most of the cell lines inoculated subcutaneously into the postauricular region of NOG mice were able to produce a large tumor very efficiently, irrespective of whether they were leukemic or in vitro transformed cells.

Comparison of ED-40515(−) cells growth in NOG and NOD-SCID mice. To assess and clarify the mechanism of in vivo tumor cell growth in NOG mice, we inoculated cells of the ED-40515(−) cell line (10^7 cells) subcutaneously into NOG mice without common γ-chain. For comparison, mice of the parent strain, NOD-SCID with common γ-chain, were also used. Three NOD-SCID and three NOG mice were sacrificed 1 week as well as 2 weeks after inoculation. Results showed that there was significant difference in successful engraftment of tumor cells in an individual mouse of both strains. In the case of NOG mice the number of cells increased from initial level by about 7.6 and 23.6-fold on day 8 and 15, respectively. In control NOD-SCID mice, the number of inoculated cells was decreased by about 4.59- and 2.73-fold on day 8 and 15, respectively (Fig. 2). The common γ-chain is a critical molecule for the development of T and NK cells (6, 13). In addition, a defect of dendritic cell function was reported (13). Thus, these results suggest that NK deficit or functional defects in dendritic cells are responsible for the production of a progressively growing large tumor in NOG mice.

Infiltration of HTLV-1-infected cell lines into the different

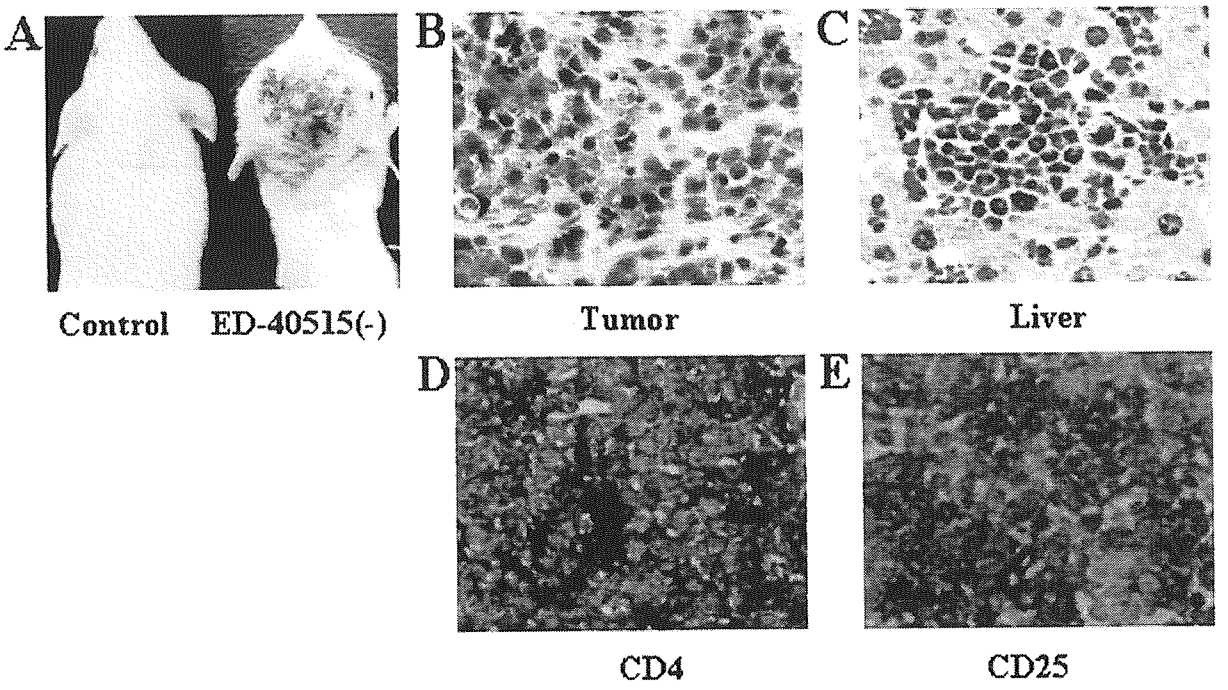

FIG. 1. Tumor growth and infiltration in NOG mice. (A) Photographs of normal NOG mice and those inoculated with ED-40515(−) cells subcutaneously in the postauricular region after 3 weeks. H&E staining of tumor tissue of an ED-40515(−) injected mouse (B) and a section of the tumor-bearing liver of an SLB-1-inoculated mouse (C). In vivo expression of CD4 and CD25 are revealed by immunohistochemistry. Immunohistochemical staining using anti-CD4 (D) and anti-CD25 (E) was conducted on tumor tissues from mice 2 weeks after inoculation of the ED-40515(−) cell line.

organs of NOG mice. To assess the tissue distribution of HTLV-1-infected cell lines, we carried out histological examinations of the different organs of NOG mice inoculated with different types of cell lines (Table 2). Inoculation of HTLV-1-infected cell lines led to progressive tumor formation at the inoculated site and infiltration into peripheral circulation. Proliferation and infiltration of tumor cells were found not only in primary tumor tissues, but also in peripheral blood, bone marrow, lung, liver, spleen and kidney of NOG mice inoculated with the ED-40515(−) cell line. Additionally, the heart and brain were also involved in NOG mice inoculated with the SLB-1 cell line. We also found that mice inoculated with Hut-102, MT-1 and TL-Oml cell lines exhibited infiltration in various organs in a similar manner as that of leukemia, eventually resulting in death. H&E staining showed a massive infiltration of tumor cells at the site of inoculation with ED-40515(−) and in the liver inoculated with the SLB-1 cell line (Fig. 1B and C, respectively). These data suggest that HTLV-1-infected cell lines could invade different organs of SCID mice in a leukemic manner, irrespective of their origin. Interestingly, Tax-positive in vitro transformed cell lines appeared to infiltrate the various organs of mice more aggressively and massively than leukemic cell lines.

Expression of surface proteins in the tumor tissues in mice inoculated with HTLV-1-infected cell lines. To investigate protein expression of T-cell surface antigens by immunohistochemistry, cytospin samples of in vitro culture cells and tissue sections from the tumor of mice inoculated with the

TABLE 2. Infiltration of leukemic cells into different organs of SCID mice[a]

Cell line	Infiltration of leukemic cells into:								
	Tumor	Peripheral blood	Bone marrow	Liver	Spleen	Lung	Brain	Kidney	Heart
ED-40515(−)	+++	++	±	+	+	+	±	+	−
SLB-1	+++	+++	++	+++	++	+++	+	+	+
MT-1	+++	++	−	+	+	+	+	−	−
TL-oml	+++	++	−	+++	+	±	−	−	−
Hut-102	+++	++	+++	+++	+++	+	±	−	−
MT-2	++	+	±	±	+	±	−	+	−
MT-4	++	+	±	−	+	−	−	−	−
M8116	+	±	−	−	−	−	−	−	−
TY8-3/MT-2	+	−	−	−	−	−	−	−	−

[a] Mice were injected with 1×10^7 to 7.5×10^7 cells per mouse. Tumor tissue and organ samples were examined by histological analysis. Symbols: +, slight infiltration; ++, marked infiltration; +++, massive infiltration; ±, slight or no infiltration, depending on each mouse; −, no infiltration.